Faculty of Science and Engineering

School of Earth and Planetary Science

A Novel Platform and Workflow for Underwater Photogrammetry Surveys

Alaa Anas Mufti

(0000-0002-0248-8340)

This thesis is presented for the Degree of

Doctor of Philosophy

of

Curtin University

January 202

Declaration

I, Alaa Anas Mufti, declare that to the best of my knowledge and belief, this thesis contains no material previously published by any other person except where due acknowledgment has been made.

This thesis contains no material which has been accepted for the award of any other degree or diploma in any university.

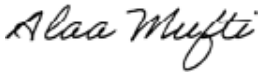

Signature:

Date: 1/1/2024

Acknowledgments

In the name of Allah, the Almighty God, the Most Gracious, and the Most Merciful, I express my deepest gratitude for blessing me with the gift of life and good health, strength, capability, and patience throughout this transformative journey.

I extend my sincere appreciation to the individuals and institutions whose contributions have been indispensable in the completion of my Ph.D. journey.

First, I express my deepest gratitude to Dr. Iain Parnum, my supervisor, for his unwavering support, insightful guidance, and invaluable mentorship throughout my research. His expertise and commitment have been instrumental in shaping the direction and quality of my work.

I would like to acknowledge the significant contributions of Co-Supervisor Dr. David Belton. His scholarly input, constructive feedback, and collaborative spirit have greatly enriched the depth and scope of my research, contributing to its overall excellence.

A special mention goes to Associate Professor Petra Helmholz, whose mentorship and academic guidance have played a crucial role in refining my research methodologies and approaches. Her expertise has been an asset to my academic journey.

I am grateful to the Saudi Arabia Cultural Mission (SACM) for their generous funding, without which this Ph.D. endeavour would not have been possible. Their commitment to supporting education has been a driving force behind my academic growth and achievements.

I extend my appreciation to King Abdulaziz University for providing the opportunity to pursue doctoral studies. The university's commitment to fostering an environment conducive to research and academic excellence has greatly contributed to my educational experience.

To my friends, I offer my heartfelt thanks for their encouragement, camaraderie, and understanding during the challenging phases of my academic pursuit. Their support has been a source of motivation and resilience.

I owe a debt of gratitude to my family for their unwavering support, and encouragement. Their belief in my capabilities has been a constant source of inspiration, and I am profoundly thankful for their presence throughout this journey.

Lastly, I sincerely thank my wife and child for their patience, understanding, unwavering support, and sacrifices. Their love and encouragement have been the bedrock of my perseverance through the highs and lows of this academic endeavour.

Each of you has played an integral role in this academic achievement, and I am sincerely thankful for your collective contributions to my Ph.D. journey.

Copyright Statement

I have obtained permission from the copyright owners to use any third-party copyright material reproduced in the thesis (e.g. questionnaires, artwork, unpublished letters), or to use any of my own published work (e.g. journal articles) in which the copyright is held by another party (e.g. publisher, co-author).

Signature: 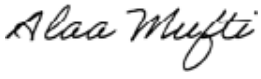

Date: 1/1/2024

List of Publications

Chapter 2: Introduction and validation of a novel calibration frame

Mufti, A., Parnum, I., Belton, D., & Helmholz, P. (2023). Introduction and validation of a novel calibration frame. International Archives of the Photogrammetry, Remote Sensing & Spatial Information Sciences, II WG II/7.

Chapter 3: An open-source, data-logging device for marine-based surveys

Mufti, A., Parnum, I., Belton, D., & Helmholz, P. (2023). An open-source, data-logging device for marine-based surveys. International Archives of the Photogrammetry, Remote Sensing & Spatial Information Sciences, II WG II/7.

Chapter 4: A novel platform and workflow for underwater photogrammetry surveys

Mufti, A., Helmholz, P., Belton, D., Allahvirdi-Zadeh, A., & Parnum, I. (2024). A novel platform and workflow for underwater photogrammetry surveys. International Annals of the Photogrammetry, Remote Sensing & Spatial Information Sciences, Midterm-symposium commission IV, submitted, decision pending.

Appendix A: Investigation of in-field devices for underwater surveying of reef structures:

Mufti, A., Parnum, I., Belton, D., & Helmholz, P. (2019). Investigation of in-field devices for underwater surveying of reef structures. Poster presented at the Australian Marine Science Association conference, Fremantle, Western Australia, 7-11 July 2019.

Abstract

Observation, monitoring, and understanding of the marine environment, particularly seafloor mapping, allows for effectively managing these important regions. Mapping the marine environment has traditionally been carried out via aerial and satellite remote sensing, or vessel-based echosounder surveys. More recently, underwater photogrammetry has gained popularity for creating three-dimensional (3D) maps and photomosaics of marine environments. However, achieving high accuracy in the geolocation and scale of underwater models generated from photogrammetry can be more challenging than terrestrial environments. This is because calibration and positioning methods are more difficult for underwater surveys, which can mean the interior and exterior orientation parameters are not adequately calculated. This thesis aims to address these two issues by developing: a camera calibration frame, and a survey platform to deploy cameras and collect ancillary data, that are more suited to underwater photogrammetry surveys. The calibration frame developed as part of this thesis was a collapsible, pyramid shape. By being collapsible, it makes the frame easy to transport and handle, which is more practical for marine field data capture. The calibration frame was validated in-air and underwater. In the underwater performance test, it achieved root-mean-squared (RMS) error values of below 2 mm when using baselines, verified that the frame is usable. The photogrammetry survey platform developed as part of this Thesis used a Raspberry Pi to collect time-synchronised ancillary data to tag images with, including: position (from a GNSS receiver), depth down from the surface (using a pressure sensor), altitude from the seafloor (using an echosounder), and motion, all deployed on a rigid frame which can have cameras mounted so they were below the water surface. The position can be processed to get the Post Processed Kinematic (PPK) position, in validation tests the RMS X-Y location was found to be between 10 and 30 cm. The seafloor depth point cloud generated from the platform was found to have an RMS with historic bathymetry data between 28 and 44 cm. The final part of the Thesis used the camera calibration frame and survey platform, to conduct an underwater photogrammetry survey of an area with artificial reef structures. To evaluate the survey performance, the resulting 3D models and photomosaics of these artificial reefs were compared to bathymetric multibeam survey data and aerial photos of the area. It was found that when using PPK data, the geolocation of the photogrammetry mosaics and 3D models was within 30-50 cm of the multibeam and/or aerial photo. The accuracy of the 3D models from photogrammetry increased: when using a pre-calibration with a frame (compared to software self-calibration) by 36%, reducing the RMS error from 27.78 cm to 17.91 cm; by tagging photos with the PPK position data

by 55%, reducing the RMS error from 18.65 cm to 8.31 cm; and with the addition of the single beam depth point cloud, notably improved the alignment of the Shift z parameter, experiencing a reduction from 20.7 cm to 8.4 cm. It is recommended that further study looks to integrate and test sensors and GNSS solutions that can offer even greater accuracy. In conclusion, this study has demonstrated a cost-effective and efficient marine research and mapping solution, that can enable a deeper understanding of the marine environment.

Contents:

List of Figures

List of Tables

Abbreviations and terminology

Terms	Abbreviations
RMSE	Root mean square error
RMS	Root mean square
LIDAR	Light Detection and Ranging
MBES/Multibeam Echosounder	Multibeam Echosounder System
echosounder, Echosounder, echo-sounder	Echosounder System
ASV	Autonomous Surface Vehicle
PPP	Precise Point Positioning
PPK	Post Processed Kinematic
RTK	Real Time Kinematic
AHD	Australian Height Datum
CC	Context Capture

Chapter 1: General Introduction

1.1 Motivation of study

The marine environment worldwide is coming under increasing pressure from human activities; including fisheries, and the increase of competition among industries for marine resources, such as oil and gas (Beaman & Harris, 2005; Manoukian et al., 2011; Pickrill & Todd, 2003). Evaluating the impacts of anthropogenic disturbances requires maps of the seafloor and underwater environment (Kostylev et al., 2001). For instance, in recent years, the mapping and monitoring of coral reefs have become highly relevant in understanding how they recover from damage over time and how they may be further damaged from human-related or natural impacts (Hedley et al., 2016). Creating benthic habitat maps would help management objectives, including detecting environmental changes, creating sampling strategies, and outlining zoning strategies (Pittman et al., 2009). However, Pickrill and Kostylev (2007) noted there is usually a lacking of high-quality information on marine ecosystems compared to their terrestrial counterparts; this is usually because it can be technically and economically prohibitive to collect the required information, such as topography. Recent advancements of underwater survey methods, such as photogrammetry and laser, show great promise as technological solutions to mapping seafloor structures in high-resolution, but there is a lack of studies understanding how these compare technically and economically with more traditional methods, such as hydroacoustic. This study investigated how different underwater surveying techniques can complement each other towards seafloor mapping applications.

1.2 Seafloor mapping techniques

There are several techniques used for surveying the seafloor (Missiaen et al., 2017). These survey techniques can be grouped up into three main types: physical surveys, on-water (in-field), and off-water (off-field) (Sabol et al., 2002). Table 1.1 summarises the advantages and disadvantages of these main methods for underwater surveying, and Figure 1.1 shows some similarities and differences between off and on water surveying techniques.

Physical surveys or *in situ* sampling techniques can be described as direct methods of sampling and observing the seafloor by using grabs, videos, and imagery. For instance, for measuring the coral reef growth a tape and line method is sometimes used. These methods produce highly detailed data with high levels of accuracy—on a very small area. However, these methods require heavy labor to operate, their area coverage is limited (Brown et al., 2011; Sabol et al., 2002).

Off-water remote sensing techniques primarily use the electromagnetic spectrum, e.g. hyperspectral imagery. The images can be obtained from either airborne or satellite sensors, and can be active or passive systems. These techniques work well under ideal conditions; however, they can be easily affected by uncontrollable factors like clouds, rough water, and low water clarity (Figure 1.1) (Sabol et al., 2002). Off-water techniques can provide large area coverage and an acceptable degree of accuracy in bathymetry mapping (Malthus & Mumby, 2003). Therefore, they are capable of developing large-scale bathymetry maps that are also cost-effective (Figure 1.1). One drawback is that aerial and satellite remote sensing techniques are typically restricted to shallow and clear coastal waters due to the limited penetration of light through seawater (Figure 1.1). In addition, when it comes to mapping small features, field surveys usually surpass off-water in resolution (Brown et al., 2011).

On-water remote sensing techniques, are usually based on the use of optical or hydroacoustic sensing devices on ships or underwater vehicles (Sabol et al., 2002). Hydroacoustic systems, such as multibeam echo-sounders, offer an effective method for creating 3D maps (Lamarche et al., 2016). However, one major disadvantage is their reduced coverage (and therefore increase in cost) in surveying shallow water structures, particularly less than 10 m deep (Figure 1.1) (Hedley et al., 2016). Optical methods are usually deployed on underwater vehicles and can be divided into passive (photogrammetry) and active (laser) systems. However, they have reduced coverage compared to multibeam echo-sounders and when deployed on an underwater vehicle can introduce additional challenges in 3D mapping, such as solving for localisation and positioning (Figure 1.1).

Table 1. 1. Diagram showing the wide range of technologies involved surveying

Methods	Advantage	Disadvantage
Physical surveys	- Produce highly detailed data with high levels of accuracy	- Require heavy labour to operate - Area coverage is limited - Difficult to produce an accurate detailed map
Off-water remote sensing	- Work well under ideal conditions - Can create different levels of coverage of an area - Provide an acceptable degree of accuracy - Cost-effective	- Can be easily affected by uncontrollable factors like clouds - Only work in shallow and coastal waters
On-water remote sensing	- Best method for creating high quality habitat maps	- Reduced coverage in surveying shallow water that is less than 5m - Increase in cost

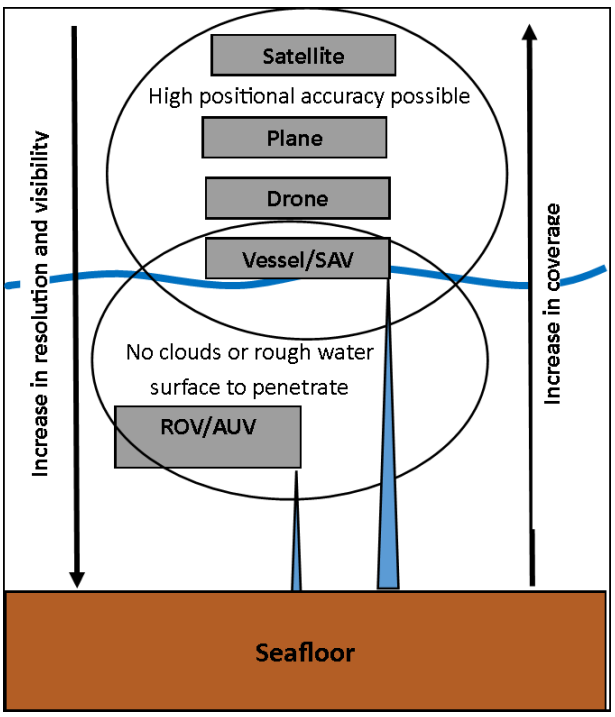

Figure 1.1: Comparison of off and on water seafloor surveying techniques.

1.2.1 Hydroacoustic surveys

Hydroacoustic systems offer an effective method for creating accurate, broadscale seafloor maps (Lurton, 2010). Three of the most used hydroacoustic systems that are currently available that can map and monitor the seafloor are single beam echosounders (SBES), side-scan sonars, and Multibeam Echosounders (MBES) (Kenny et al., 2003). Sidescan sonars are useful at identifying objects and the substrate type on the seafloor, but are not designed to measure the depth, like echosounders. The first echosounders to be utilised for bathymetry surveys were SBES, they operate by transmitting a sound wave towards the seafloor, and then use the two-way travel time (TWTT) to calculate the depth (Lurton, 2010). SBESs are still used today, as they are affordable and coupled with high-resolution GNSS can collect accurate bathymetry data. The main drawback of SBESs is they only collect depth soundings directly below the vessel, which leads to a low spatial resolution map. Whereas, MBESs systems allow survey vessels to produce high spatial resolution coverage of wide swaths of the seafloor in less ship time (Instruments, 2000), meaning large areas can be mapped relatively fast and with high precision (Missiaen et al., 2017). MBES work by forming a fan-shaped transmission of a sound wave directed at the seabed that is a Wide across-track and narrow along track, in addition to measuring the TWTT to determine range, the receive transducer array carries out beam forming to determine the angle of arrival, the result is a series of depth sounds across the vessel track (Lurton, 2010). To obtain accurate depth measurements and positions calculations of the motions made by the ship (roll, heave, heading, and pitch) are gathered using a motion sensor (Buchanan et al.). Two factors control the bathymetric potential of the MBES's target resolution capability: the differences in distance between the along-track and the across-track soundings and the size of the MBES's footprint (Kenny et al., 2003). The backscatter strength recorded by MBES can also be used to help infer seafloor substrates (Parnum & Gavrilov, 2012).

As part of this study, Mufti et al., (2019) Appendix (A) evaluated the use of MBES to create an accurate and precise image of the Artificial Reefs (AR) which dimensions are well understood through engineering diagrams. Following a survey of the area using an R2Sonic 2024 MBES, processing of the bathymetry was carried out in QPS QIMERA, including the addition of the Smoothed Best Estimate of Trajectory (SBET) files processed from the Applanix POS MV Position and Motion data. From the result obtained, it can be clearly seen that the MBES can easily show depth and object location of the ARs.

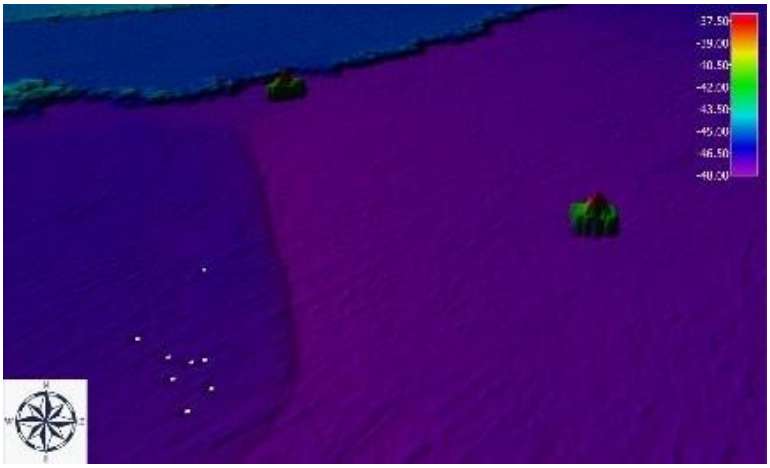

Figure 1.2: 3D View of the bathymetry image of the Artificial Reefs.

The point cloud that was obtained from MBES of the AR, was compared with the engineering diagrams Figure 1.2 and Figure 1.3. While the MBES point cloud data shows the outline of the AR, without prior knowledge of the structure it would be challenging to reconstruct the 3D structure (Figure 1.2). The backscatter data of the AR was investigated but it did not provide any addition information (Mufti, 2019) . What would help in understanding the structure of the AR would be having imagery taken at the same time.

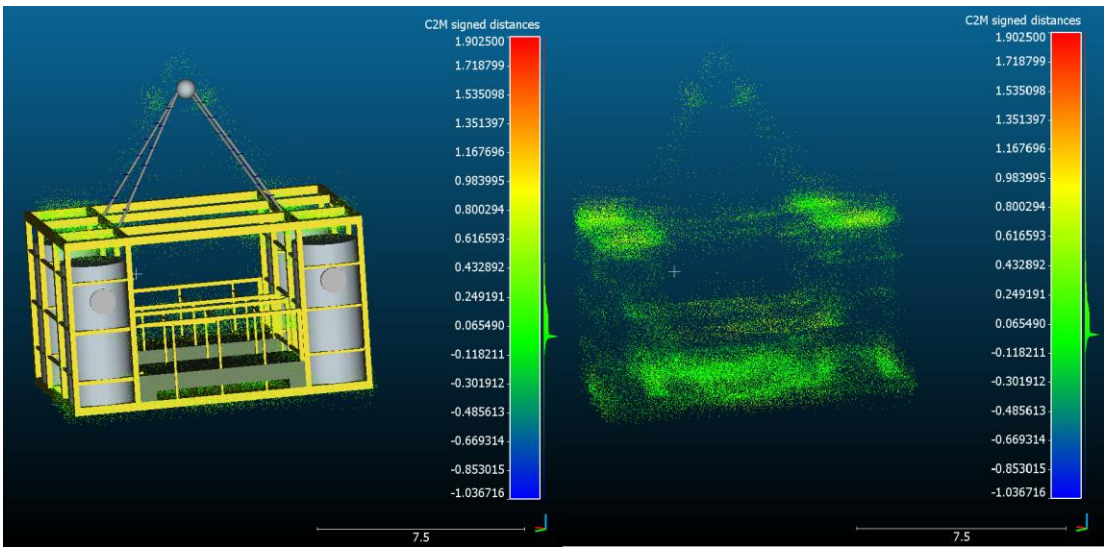

Figure 1.3: The multibeam point cloud and the diagram of AR tower (left), and signed distance between the multibeam point cloud and the diagram of AR tower (right).

1.2.2 Underwater photogrammetry

Photogrammetry is a simple technique with a low cost that can provide 3D models of the seafloor (Drap, 2012). Aerial based photogrammetry (including drones), have been successful at mapping shallow waters (Agrafiotis et al., 2020), but capturing images above the water can be challenging and require both clear water but a low sea state (Woodget et al., 2015). Imagery of the seafloor is clearer and at a higher resolution when taken underwater than above it (Figure 1.1). Underwater Photogrammetry was first used in the 1960s and 1970s in documenting underwater archaeology and it was achieved by using pairs of aerial stereo cameras being adapted to underwater conditions (Balletti et al., 2015). The underwater photogrammetry technique is no different than the traditional one, but it is important to address some elements that can cause disturbance, such as light refraction effects, which may happen due to camera housing and the two-media boundary (Gawlik, 2014).

One key aspect to a successful photogrammetry survey is camera calibration (Luhmann et al., 2016). Previous studies can be categorised in to two types: ones that use "self-calibration" carried out by photogrammetry software (Kılınç Kazar, 2022), one that carry out a dedicated "pre-calibration", normally using a frame with known control points (Helmholz et al., 2016; Shortis et al., 2000). Using a calibration frame in an underwater setting can be challenging as they are usually bulky and not easy to handle.

One of the drawbacks of using photogrammetry to survey the seafloor is that it requires good visibility, and so they are usually deployed on an underwater vehicle, and while the closer the camera is to the target, the higher the resolution, this does reduce the coverage (Figure 1.1). Moreover, if cameras are deployed on underwater vehicles, it presents challenges in positioning and navigation, as GNSS methods can be used. Positioning underwater is most commonly done with acoustic methods such as Long baselines, short baselines and ultra-short baseline, which require significant more costs and technical challenges to come close to the accuracy and reliability of GNSS methods (Wu et al., 2019). In the terrestrial domain, poor positioning can sometimes be compensated for with enough Ground-Control Points (GCPs); however, creating underwater GCPs can be significantly challenging and not a trivial exercise (Missiaen et al., 2017).

1.3 Related work

Numerous commercial devices demonstrate the ability to collect data for depth and position simultaneously, yet certain limitations, such as high costs and insufficient adaptability. Despite the existence of open-source platforms tailored for similar applications, the specific criteria of the study remained unmet by other alternatives that will be discussed.

In contrast, a novel platform specifically designed for underwater photogrammetry surveys stands out. An Autonomous Surface Vehicle (ASV) not only fulfills the study's criteria but also extends its utility to the collection of environmental data. Engineered to be cost-effective, the ASV boasts adaptability, providing a flexible foundation for the seamless integration of additional sensors, further enhancing its capabilities for comprehensive underwater photogrammetry surveys.

Addona et al. (2022) presents a comparative study on coastal monitoring, featuring a low-cost Raspberry Pi-based camera system named VISTAE. This research aligns with the concept of open-source, data-logging devices for marine-based surveys, emphasizing the advantages of such technologies in coastal vulnerability assessments. The study's integration of field measurements and remote observations using VISTAE highlights the potential for Raspberry Pi or similar devices in enhancing coastal monitoring capabilities. This supports the broader application of open-source solutions in marine research, aligning with the principles advocated in the development of an open-source, data-logging device for marine-based surveys using Raspberry Pi.

Vargas et al. (2023) presents EMAC-USV, a modular, low-cost, open-source Unmanned Surface Vessel for monitoring bathymetry and water quality. This aligns with the principles of open-source, data-logging devices for marine surveys using Raspberry Pi, emphasizing cost-effectiveness and adaptability. Both initiatives showcase the trend in using accessible technology for efficient environmental data collection, with EMAC-USV demonstrating its capabilities in waste stabilization ponds and tidal channels.

Barrile et al. (2019) work on the experimental system for acquiring and processing digital images using UAV and ROV technology contributes to the broader theme of open-source data acquisition in marine environments. The emphasis on employing a small, low-cost ROV aligns with the principles of cost-effectiveness and accessibility, which are central to open-source solutions. The idea of

constructing a 3D model of underwater structures and comparing bathymetry values resonates with the goals of innovative data-logging devices, such as the one utilizing Raspberry Pi, for marine-based surveys. Both efforts aim to enhance data collection efficiency and affordability, reflecting a shared commitment to advancing open-source approaches in marine science and technology.

Morel et al. (2022) introduces the Yellowfish autonomous surface vehicle (ASV), an open-source, data-logging device tailored for marine-based surveys and environmental research. This innovative tool, powered by a Raspberry Pi 4 model B and Navio2 for data processing and control, incorporates T200 thrusters for precise steering. The report delves into the ASV's rigid-body model, on-board electronics, and control systems, emphasizing its role in open-source data acquisition, particularly for marine pollution monitoring. The study not only details the technical aspects of the Yellowfish ASV but also underscores its significance within the realm of open-source initiatives aimed at enhancing accessibility to advanced tools for environmental data collection.

Bibuli (2021) introduced a groundbreaking methodology for underwater photogrammetry surveys using the Shallow Water Autonomous Multipurpose Platform (SWAMP), an Autonomous Surface Vehicle (ASV) designed for challenging river conditions. The study demonstrated SWAMP's high maneuverability and adaptability in navigating shallow waters, successfully collecting bathymetric data in the Roja River, West Liguria. The research highlights the potential of ASVs, like SWAMP, to enhance the quality and spatial resolution of surveys in challenging aquatic environments. Future work aims to integrate bathymetric data with photogrammetric information obtained by aerial drones, further advancing underwater environmental monitoring.

Kawamura et al. (2021) introduce a novel autonomous surface vehicle (μ-ASV) for underwater photogrammetry surveys, addressing challenges in conventional ASVs. The microASV, a compact surfboard-based vessel, employs sliding mode control for waypoint navigation and dynamic positioning system (DPS) control. Experimental results show successful autonomous navigation, but limitations include potential model errors and disturbances overlooked by the control method. The study highlights applications in aquaculture and coastal research, emphasizing the μ-ASV's potential for various scenarios, despite its limitations.

Łubczonek (2022) f ocusing on a case study in Lake Dabie, Poland, the research employs Unmanned Aerial Vehicles (UAVs) and Unmanned Surface Vehicles (USVs) to enhance understanding of

underwater environments. Utilizing a DJI Phantom Pro surveying platform, the investigation centers on a bay in Lake Dabie for photogrammetric data acquisition. Despite challenges related to poor water transparency limiting effective data acquisition to 1.3 meters, the study addresses this with an innovative solution. Integration of hydroacoustic methods, employing a USV with a Single-Beam Echo Sounder (SBES) sensor, enhances data collection. The research underscores the importance of integrating classical photogrammetry and hydroacoustic techniques to overcome constraints in underwater data collection, emphasizing the significance of such integrative methodologies in advancing research.

Rubio (2023) provides valuable insights by comparing Multibeam Echosounder on a USV with traditional photogrammetry for documenting shallow-water cultural heritage sites in the Bay of Algeciras. This work delves into the efficacy, precision, and practical applicability of both methods in underwater archaeological contexts, offering a comprehensive exploration of their advantages and limitations. The study significantly contributes to shaping best practices in preserving, documenting, and monitoring such sites. Despite acknowledging inherent limitations, Rubio's research presents nuanced perspectives that guide researchers and practitioners in navigating the complexities of underwater cultural heritage documentation. It sheds light on suitable techniques, trade-offs, and associated challenges, providing informed viewpoints for the field.

Abadie (2018) highlights the rising importance of georeferenced underwater photogrammetry in mapping marine habitats and submerged structures. The technique involves precise underwater image capture and advanced georeferencing, providing unmatched accuracy in situating images geographically. This study underscore its pivotal role in ecological research, offering detailed maps for understanding marine ecosystems and supporting conservation. However, limitations include challenges in capturing images in murky waters and the need for sophisticated equipment. The study emphasizes its versatility in documenting submerged structures, contributing to the preservation of underwater cultural heritage. Despite its transformative potential, considerations of underwater visibility and equipment accessibility present challenges. The fusion of advanced imaging and geospatial precision positions georeferenced underwater photogrammetry as a transformative tool, with considerations for limitations, facilitating a comprehensive exploration of the underwater landscape.

Rofalski (2020) investigates integrating ROV-based photogrammetric underwater imagery with multibeam soundings for reconstructing wrecks in turbid waters. Addressing challenges of reduced

visibility, the study explores synergies between photogrammetry and multibeam sonar technology. By combining these methods, it aims to enhance accuracy and completeness in wreck reconstructions, offering insights into submerged archaeological sites. This fusion presents a promising approach for overcoming turbid water limitations, providing a novel perspective on underwater cultural heritage documentation. However, challenges include potential data distortion in turbid conditions and the need for specialized equipment

1.4 Thesis objectives and structure

As discussed above, the use of both optical and hydroacoustic systems have been widely used for seafloor mapping applications; however, each system has its own advantages and limitations (Lubczonek et al., 2021; Roman et al., 2010). Hydroacoustic systems can be used to collected accurate and reliable bathymetric data, but require expensive systems, like MBES, to collect high resolution data, and while it could produce backscatter data to infer substrate, it is not the same level of detail as a photograph (Figure 1.3). On the other hand, photogrammetry can readily create a high detailed 3D models that include colour information (Shortis et al, 2016); however, aerial based photogrammetry of the seafloor will struggle for GCPs and penetration of the water surface (Figure 1.1 and Figure 1.3), and underwater photogrammetry improves the imagery but at the expensive of less reliable positioning (Figure 1.3). This study aimed to create accurately scaled and georeferenced 3D maps and orthomosaics of the seafloor, by combining the advantages of an underwater photogrammetry platform with an on-water hydroacoustic bathymetry surface platform (Figure 1.1). Specifically, this study aimed to create a surface platform that was able to deploy cameras below the water line, to remove effects of clouds and the sea surface (like waves), on a fixed reference frame of an hydroacoustic on-water platform that collected GNSS and depth data that can be used to constraint images in the photogrammetry workflow (Figure 1.1). In addition, the study aimed to create the survey platform using an open-source and cost-effective tool (namely a by using Raspberry Pi) to collect data to make it more accessible to others to replicate (Figure 1.3). While other studies have proposed and/or investigated similar data fusion themes, this study hopes to progress this promising area further (Ferreira, 2016). The objectives of this Thesis are:

- Objective 1: Evaluate the use of multibeam and underwater photogrammetry (this chapter).
- Objective 2: Development of a portable calibration frame for underwater photogrammetry surveys (Chapter 2).
- Objective 3: Development of a low cost, open-source acquisition system and platform to

support underwater photogrammetry surveys (Chapter 3).

- Objective 4: A novel workflow and platform for carrying out underwater photogrammetry surveys (Chapter 4).
- Objective 5: Assessment of the success and limitations of the study (Chapter 5).

Chapter 2 and 3 were presented and published as papers at the International Society for Photogrammetry and Remote Sensing Geospatial week conference Cairo September 2023. Chapter 4 is in draft form ready for submission.

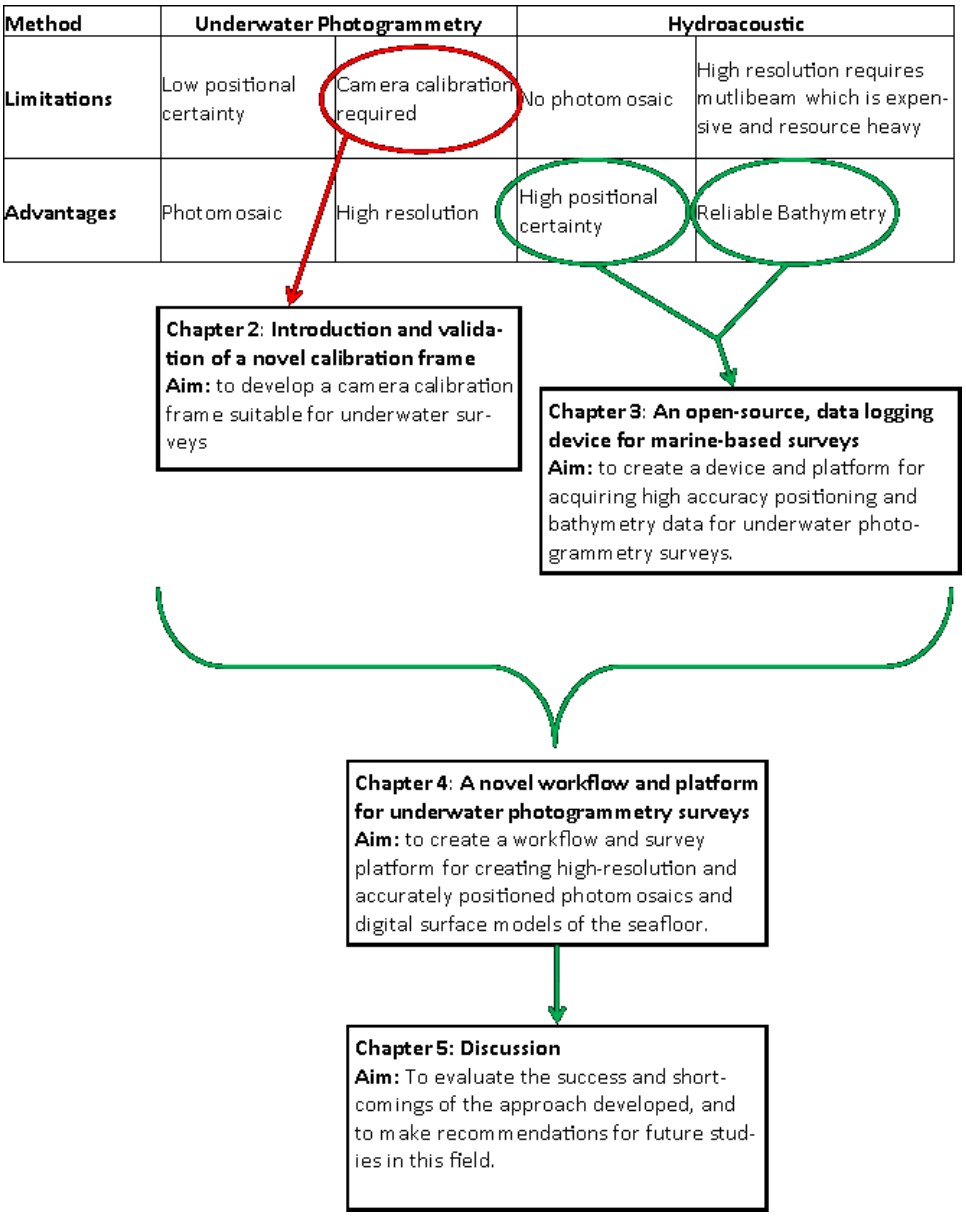

Figure 1.4: Advantages and limitations of underwater photogrammetry and hydroacoustic surveys of the seafloor combined with the thesis structure.

References

Abadie, A., Boissery, P., & Viala, C. (2018). Georeferenced underwater photogrammetry to map marine habitats and submerged artificial structures. The Photogrammetric Record, 33(164), 448-469.

Agrafiotis, P., Karantzalos, K., Georgopoulos, A., & Skarlatos, D. (2020). Correcting image refraction: Towards accurate aerial image-based bathymetry mapping in shallow waters. *Remote Sensing, 12*(2), 322.

Balletti, C., Beltrame, C., Costa, E., Guerra, F., & Vernier, P. (2015). Underwater Photogrammetry and 3D Reconstruction of Marble Cargos Shipwreck. *International Archives of the Photogrammetry, Remote Sensing & Spatial Information Sciences*.

Beaman, R. J., & Harris, P. T. (2005). Bioregionalization of the George V Shelf, East Antarctica. *Continental Shelf Research, 25*(14), 1657-1691.

Bibuli, M., Ferretti, R., Odetti, A., & Cosso, T. (2021). River Survey Evolution by means of Autonomous Surface Vehicles. 2021 International Workshop on Metrology for the Sea; Learning to Measure Sea Health Parameters (MetroSea),

Brown, C. J., Smith, S. J., Lawton, P., & Anderson, J. T. (2011). Benthic habitat mapping: A review of progress towards improved understanding of the spatial ecology of the seafloor using acoustic techniques. *Estuarine, Coastal and Shelf Science, 92*(3), 502-520.

Buchanan, C., Spinoccia, M., Picard, K., Wilson, O., Sexton, M., Hodgkin, S., Parums, R., Carey, M., & Siwabessy, J. Standard Operation Procedure for a Multibeam Survey.

Drap, P. (2012). Underwater photogrammetry for archaeology. *Special applications of photogrammetry*, *114*.

Gawlik, N. (2014). *3D modelling of underwater archaeological artefacts* Institutt for bygg, anlegg og transport].

Hedley, J. D., Roelfsema, C. M., Chollett, I., Harborne, A. R., Heron, S. F., J. Weeks, S., Skirving, W. J., Strong, A. E., Eakin, C. M., & Christensen, T. R. (2016). Remote sensing of coral reefs for monitoring and management: a review. *Remote Sensing, 8*(2), 118.

Helmholz, P., Long, J., Munsie, T., & Belton, D. (2016). ACCURACY ASSESSMENT OF GO PRO HERO 3 (BLACK) CAMERA IN UNDERWATER ENVIRONMENT. *International Archives of the Photogrammetry, Remote Sensing & Spatial Information Sciences, 41*.

Kawamura, Y., Tahara, J., Kato, T., Fujii, S., Baba, S., & Koike, M. (2021). Development of small autonomous surface vehicle implementing position control system using sliding mode control. *Sens Mater, 33*(3), 883-895.

Kenny, A. J., Cato, I., Desprez, M., Fader, G., Schüttenhelm, R., & Side, J. (2003). An overview of seabed-mapping technologies in the context of marine habitat classification. *ICES Journal of Marine Science, 60*(2), 411-418.

Kılınç Kazar, G., Karabörk, H., & Makineci, H. B. (2022). Evaluation of test field-based calibration and self-calibration models of UAV integrated compact cameras. *Journal of the Indian Society of Remote Sensing, 50*(1), 13-23.

Kostylev, V. E., Todd, B. J., Fader, G. B., Courtney, R., Cameron, G. D., & Pickrill, R. A. (2001). Benthic habitat mapping on the Scotian Shelf based on multibeam bathymetry, surficial geology and sea floor photographs. *Marine Ecology Progress Series, 219*, 121-137.

Lamarche, G., Orpin, A. R., Mitchell, J. S., & Pallentin, A. (2016). Benthic habitat mapping. *Biological sampling in the deep sea*, 80-102.

Lubczonek, J., Kazimierski, W., Zaniewicz, G., & Lacka, M. (2021). Methodology for combining data acquired by unmanned surface and aerial vehicles to create digital bathymetric models in shallow and ultra-shallow waters. *Remote Sensing, 14*(1), 105.

Luhmann, T., Fraser, C., & Maas, H.-G. (2016). Sensor modelling and camera calibration for close-range photogrammetry. *ISPRS Journal of Photogrammetry and Remote Sensing, 115*, 37-46.

Malthus, T. J., & Mumby, P. J. (2003). Remote sensing of the coastal zone: an overview and priorities for future research.

Manoukian, S., Fabi, G., & Naar, D. F. (2011). Multibeam investigation of an artificial reef settlement in the adriatic sea (Italy) 33 years after its deployment. *Brazilian Journal of oceanography, 59*, 145-153.

Missiaen, T., Sakellariou, D., & Flemming, N. C. (2017). Survey strategies and techniques in underwater geoarchaeological research: An overview with emphasis on prehistoric sites. *Under the sea: Archaeology and palaeolandscapes of the continental shelf*, 21-37.

Parnum, I., & Gavrilov, A. (2012). High-frequency seafloor acoustic backscatter from coastal marine habitats of Australia. *Proceedings fo the Australian Society of Australia*.

Pickrill, R. A., & Todd, B. J. (2003). The multiple roles of acoustic mapping in integrated ocean management, Canadian Atlantic continental margin. *Ocean & Coastal Management, 46*(6-7), 601-614.

Pittman, S. J., Costa, B. M., & Battista, T. A. (2009). Using lidar bathymetry and boosted regression trees to predict the diversity and abundance of fish and corals. *Journal of Coastal Research*(10053), 27-38.

Roman, C., Inglis, G., & Rutter, J. (2010). Application of structured light imaging for high resolution mapping of underwater archaeological sites. OCEANS'10 IEEE SYDNEY,

Sabol, B. M., Eddie Melton, R., Chamberlain, R., Doering, P., & Haunert, K. (2002). Evaluation of a digital echo sounder system for detection of submersed aquatic vegetation. *Estuaries, 25*(1), 133-141.

Shortis, M. R., Miller, S., Harvey, E., & Robson, S. (2000). An analysis of the calibration stability and measurement accuracy of an underwater stereo-video system used for shellfish surveys. *Geomatics Research Australasia*, 1-24.

Woodget, A., Carbonneau, P., Visser, F., & Maddock, I. P. (2015). Quantifying submerged fluvial topography using hyperspatial resolution UAS imagery and structure from motion photogrammetry. *Earth surface processes and landforms, 40*(1), 47-64.

Chapter 2: Introduction And Validation of a Novel Calibration Frame

This chapter addresses the challenges of using photogrammetry in marine environments by introducing a collapsible and portable calibration frame. The frame undergoes rigorous validation, demonstrating minimal bias, consistent results across software and cameras, enhancing data accuracy for underwater application. This innovation provides a versatile solution for field data capture in marine science.

Method	**Underwater Photogrammetry**		**Hydroacoustic**	
Disadvantages	Low positional certainty	Camera calibration required	No photomosaic	High resolution requires mutlibeam which is expensive and resource heavy
Advantages	Photomosaic	High resolution	High positional certainty	Reliable Bathymetry

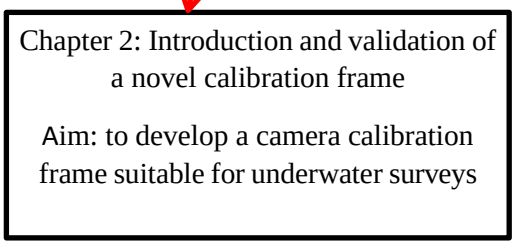

Mufti, A., Helmholz, P., Parnum, I., and Belton, D.: Introduction and Validation of a Novel Calibration Frame, *Int. Arch. Photogramm. Remote Sens. Spatial Inf. Sci.*, XLVIII-1/W2-2023, 1935–1942, https://doi.org/10.5194/isprs-archives-XLVIII-1-W2-2023-1935-2023, 2023.

INTRODUCTION AND VALIDATION OF A NOVEL CALIBRATION FRAME

A. Mufti[1,2]*, P. Helmholz [1], I. Parnum [1], D. Belton [1]

[1] School of Earth and Planetary Sciences, Curtin University
GPO Box U1987, Perth WA 6845, Australia, alaa.mufti@postgrad.curtin.edu.au, (Petra.Helmholz, I.Parnum, D.Belton)@curtin.edu.au
[2] King Abdulaziz University, Jeddah 21442, Saudi Arabia

Commission II WG II/7

KEY WORDS: Calibration, Photogrammetry, Portability, camera calibration, self-calibration

ABSTRACT:

The use of Photogrammetry is increasingly used by several disciplines, including marine science. Among others, the accuracy of a 3D model generated from images, depends on the quality of the calibration and stability of the camera used to capture the images. For the calibration an optimum 3D geometry is essential to minimise correlations between the camera's interior orientation parameters. For the calibration, usually various different types of calibration frames are used. However, in practice, it can be challenging to use these frames when working in underwater environments. Calibration frames can be bulky, which makes them difficult to handle and transport, especially in boats where space is at a premium. This study aimed to develop a collapsible (and thereby portable) calibration frame, which is more practical for marine field data capture. The proposed collapsible calibration frame is validated in-air and underwater. Overall, three tests are performed. Firstly, the reliability of the frame is validated, i.e. if the collapsible frame can be put together in such a way that the Ground Control Points (GCPs) on the frame have unchanged positions relative to each other. The test showed a very small bias which could be removed by changing to a baseline assessment. Secondly, repeatability is validated, i.e. if the same results can be achieved for different software and camera combinations when using the same baselines. The test showed a clear downwards trend of the results for lower-grad cameras. However, all adjustments using the different software solutions and cameras show that the frame is suitable for application in-air. The final test is an underwater performance test which verified that the frame is usable achieving root-mean-squared error values of below 2 mm when using baselines.

1. INTRODUCTION

In recent years, there has been an increase in the use and development of marine resources, including the growth of aquaculture, deep-sea mining, shipping, and tourism. At the same time, observation, monitoring, and understanding of the marine environment are central topics of marine research that have received worldwide attention recently (Yuan et al., 2022).

The development and improvement of camera sensors and optical components have made it possible for underwater photogrammetry to become more accessible and affordable in recent years. As a result, non-professionals can now use off-the-shelf underwater photogrammetry action cameras with waterproof housings, such as the GoPro camera, to create 3D models of underwater areas. This has opened up new possibilities for a wide range of applications, including marine biology (Jalal et al., 2020), reef mapping (Guo et al., 2016) archaeology (Diamanti et al., 2017), oceanography, and more.

Before images acquired by a camera can be utilised to retrieve geometric information of a structure, distortions in the camera and lens must be addressed (Shortis, 2019). Hence, a good and reliable 3D model result that can be generated from these action cameras depends on the calibration quality and the system's stability. For instance, the refractive index of water is different to air. It is known that the refraction index of water varies with depth, and the complete light path must be coordinated, including the camera lens, housing port, and water medium (Shortis, 2019).

Incorrect calibration parameters can create a doming effect known as the "bowing effect". This effect creates a scooping or bowing in the model's centre. This issue can be overcome or reduced by camera calibration (Samboko et al., 2022).

Hence, a properly calibrated underwater camera system is crucial for accurate and consistent 3D object measurement. One way to achieve this is through self-calibration (Fraser et al., 1995). The image quality, geometry, and redundancy of the calibration image network are critical factors that impact the reliability and precision of camera calibration in underwater photogrammetry. To ensure reliable calibration, several criteria have been proposed, including:

1. the use of three-dimensional camera and target arrays,
2. the acquisition of different convergent camera views of the targets,
3. the filling of the camera's field of view with the calibration fixture or range, and
4. the capture of different rotations of the camera(s) around the optical axis.

In practice, though, it can be challenging to meet all of these requirements, especially when working in underwater environments (Guo et al., 2016). Efforts should be made to meet as many of these criteria as possible to ensure the accuracy and reliability of the camera calibration. Therefore, usually a calibration frame is used and placed in the field of view of the camera. The diver then carries out "flying orbits" around this frame in a distance allowing to fulfil all the requirements listed

* Corresponding author

above (Helmholz et al. 2016). This procedure entails capturing multiple converging images of a calibration frame with known locations of target points such as circular dots. Alternatively, the checkerboard method is used where the target points are replaced with the corners of the checkerboard. Coded targets or image analysis techniques to automatically extract the locations of the target points such as through centroid fitting methods can improve efficiency (Shortis and Seager, 2014). The scale of the 3D measurement space is established by incorporating known distances between targets or by using the 3D coordinates relative to a target reference system.

A downside of calibration frames, is they can be bulky and difficult to handle especially underwater. This has been identified as an issue by marine scientists and the request was made to overcome this challenge. This study aims to introduce a new calibration frame, created to make it more practical for marine field data capture, and to test if the frame fulfils the photogrammetric (accuracy and repeatability).

The paper is structured as follows: in the next section, a literature review is presented to quantify the level of accuracy which is required for underwater marine photogrammetry after this, the new developed frame is introduced; this is followed by details of the methodology used to assess the frame; followed by the results of the assessment; and the paper ends with study's conclusions.

2. RELATED WORK

Calibration is a crucial component of underwater photogrammetry, because it is essential to correct for camera parameters, including distortions. In underwater photogrammetry, the significance of calibration cannot be overstated. Without precise calibration, the resulting 3D models may contain errors, which can have severe consequences for scientific research, marine conservation, and underwater engineering. For instance, if photogrammetry is used to assess the growth of coral, then distortions can skew distance observations and consequently derived growth information.

The calibration stability of underwater camera systems is highly dependent on the relationship between the camera lens and the housing port. It is crucial to rigidly mount the camera in the housing to maintain a consistent total optical path from the image sensor to the water medium. Studies have demonstrated that reliable calibration can only be achieved when the camera inside the housing is securely connected to the camera port (Shortis & Harvey, 1998; Shortis et al., 2000). Testing and validation have confirmed the importance of a rigid connection for accurate calibration.

Under optimal in-air conditions, the typical root-mean-squared error (RMS) of image observation error for control points have a range from 0.03 to 0.1 pixels (Shortis et al., 1995). However, when operating underwater, the RMS error degrades due to light attenuation, contrast loss, and minor non-uniformities in the medium, resulting in a range of 0.1 to 0.3 pixels. This degradation is a result of both increased statistical variations in image measurements and the influence of uncompensated systematic errors. In situations with poor lighting or visibility, the RMS error deteriorates rapidly (Wehkamp and Fischer, 2014).

The proportional error is another measure used to assess the calibration results of cameras. It is calculated by taking the ratio of the RMS error in the 3D coordinates of the targets to the largest dimension of the object. This indicator measures how well the camera's calibration performs, relative to the size of the object being captured. The average figure is approximately 1:5000 for underwater environments (Shortis, 2019).

Two main types of structures have been used to calibrate cameras for underwater photogrammetry: 2D checkerboards and 3D calibration frames. For instance, Bouguet (2017) used a small 2D checkerboard that had 36 squares: 18 black and 18 white. After the initial calibration, camera parameters were calculated in two subsequent steps: the initialization step and the optimization step. However, additional calibrations were required to obtain a pixel error of 0.19534. It is noteworthy, that this low error was achieved with a high-quality camera. Using a 2D checkerboard offers significant advantages, including the simplicity of the calibration fixture and the efficient measurement and processing of captured images. These benefits are achieved through the automated recognition of the checkerboard pattern (Zhang 2000), which enables swift and accurate analysis. The reliability and accuracy of measurements obtained through the checkerboard technique are constrained by the compact size and two-dimensional characteristics of the checkerboard. This method is more akin to a fixed test range calibration rather than a self-calibration, as the coordinates assigned to the checkerboard corners remain static. It is important to consider that inaccuracies in these coordinate values can significantly influence the calibration process, especially when the checkerboard deviates from a true two-dimensional plane. Such deviations have the potential to introduce systematic errors, thereby impacting the overall accuracy of the calibration results (Bouguet, 2017). In addition, the 2D checkerboard is a plane, which can lead to large correlation values between the camera calibration parameters (Shortis, 2019). For these reasons, a checkerboard was not used for this research.

Gourgoulis et al. (2008) employed a calibration frame which actually consisted of two aluminium frames: a large frame and a small frame. The dimensions of the large frame were 1m x 3m x 1m, and the dimensions of the small frame were 1m x 1m x 1m. Both frames had 32 designated points with known coordinates. In the case of the large frame, each of its eight vertical rods was marked with four points. Three of these served as control points for the calibration of the space, while the remaining fourth were used as Check Points to validate the calculations. For the small frame, six control points and two Check Points were inscribed on each of the four vertical rods. Hence, overall, both frames together carried 24 control points and 8 check points. They achieved an RMS in air for the small frame was 3.70 mm and for the large frame 4.66 mm. The RMS underwater for the small frame was 4.5 mm and the large frame was 5.92 mm.

Challis and Kerwin (1992) utilised a frame measuring 1.0 m x 0.6 m x 1.0 m, with the diminutive dimensions guaranteeing stability, to calibrate two single-lens reflex (SLR) 35 mm cameras: a Canon EOS 750 and a Canon EOS 620. The calibration structure was designed to include control locations throughout the calibration space. For the structure, twelve-millimetre-diameter steel tubing was used, with fifty 42-millimetre-diameter cylinders with central holes firmly attached. Spheres were utilised because they would be identifiable from any angle. Black matte paint was applied to the frame to reduce reflections. The frame provided a total of 51 control points, with the additional point located in the centre of the central cross. Using a laser- based surveying system, the locations of the control points were ascertained. The RMSE was 0.8 mm.

Helmholz et al. (2016) utilised a GoPro Hero 3 and an open cube calibration frame with a dimension of 60cm x 60cm x 50cm.

Along two planes, the calibration frame has 52 reference marks. 25 Ground Control Points (GCP) and 27 Check Points (CP) were randomly selected ensuring a god distribution for both sets of points. The aim of the paper was to assess the camera stability by performing different camera resolutions (7 MB and 12 MB) and different camera captured (e.g. shaking the camera between captures or removing the camera from the water tight housing between captures). The maximum RMSE from the tests carried out, was 0.45 mm for the 7 MB camera, and 2.5 mm for the 12 MB one.

Capra et al. (2015) utilised a frame made of PVC bars that form the approximate margins of a parallelepiped measuring 0.90m x 0.20 m x 0.15 m and weighing 3 kilogrammes. 34 Ground Control Points (GCP) and the targets are signalling with a 30 mm wide circles, alternately black and cross-printed rectangular target. All targets materialised on the frame have been numbered and measured, and their x, y, and z coordinates have been determined in an on-frame reference system. There were three cameras used: the Canon PowerShot G12 with an RMS of 0.524 mm, the GoPro Hero2 with an RMS of 43.037 mm, and the Intova Sport HD with an RMS of 11.33 mm. Both the GoPro Hero2 and Intova Sport HD have shown large RMS values for underwater environments. This is due to the strong distortion caused by the lenses with a very small focal length.

Li et al. (1997) used a rectangular aluminium frame with a dimension of 1.4 m x 1.4 m x 0.7 m with 24 control targets marked with highly reflective circular discs with an 8-cm diameter and a well-defined centre with an accuracy of 0.8 cm along the X and Y direction and 1.2 cm along the Z with an overall RMS of 10.83mm.

Manuscript	Frame design	GCPs/CPs	RMS
Gourgoulis et al. (2008)	large frame (1 m x 3 m x 1 m) in combination with a small frame (1 m x 1 m x 1 m)	24 GCPs 8 CPs	In air: 3.7 mm – 4.66 mm Underwater: 4.5 mm 5.92 mm
Challis and Kerwin (1992)	1.0 m x 0.6 m x 1.0 m ,	51 GCPs	0.8 mm
Helmholz et al. (2016)	60 cm x 60 cm x 50 cm	25 GCPs 27 GCPs	0.45 – 2.5 mm
Li et al. (1997)	1.4 m 1.4 m 0.7 m	24 GCPs	10.83 mm underwater
Capra et al. (2015)	0.90 m x 0.20 m x 0.15 m	45 GCPs	-Hero2: 43.03 mm -Intova Sport HD: 11.330 mm -Canon PowerShot G12: 0.524 mm

Table 1: Summary of results achieved by selected calibration frames.

In conclusion, the design of calibration frame is usually a ridged construction, with dimensions of 1 m or more, which make it challenging to transport the frame. The number of GCPs and CPs is usually around 25. All points are equally distributed. RMS of 0.5 mm – 3 mm are considered acceptable for calibration outcomes in underwater environment (Shortis et al., 1995; Helmholz et al., 2016). The RMS is impacted by the camera used, the layout and geometry used to capture the images and finally the calibration frame. This covers a wide range of applications. The aim is to achieve similar RMS value when using the proposed calibration frame. Finally, while Shortis et al., (1995) define the range of acceptable point referencing error (PRE) with 0.1 to 0.3 pixels, our experiences show that 0.5 pixels are acceptable in air and 1 pixel is acceptable underwater (Shortis et al., 1995).

3. PROPOSED FRAME

The proposed solution is a triangular pyramid shape constructed with six metal, square-shaped bars (3 cm x 3 cm x 138 cm) and four 3D-printed apex joints connected with long screws and bolts (Figure 1). The joints ensure that the frame can be ensembled again in the same shape. The design was found to be light in weight approximately 3 kg, and it can be changed into two forms: a pyramid shape used for calibration, and two cylindrical shapes (made with three bars each) that easily fit into transportation tubes. White (paper), circular GCPs (diameter of 24 mm) were stuck on the bars (Figure 1). Each bar has a total of 20 dots (four on two of the sides and six each on the other two sides), which results in a total of 120 GCPs that could potentially be used. To distinguish and orientate the different bars of the pyramid, there are labels in the middle and the end of each bar (Figure 1). However, sometimes the labels may become blurred and difficult to read underwater, especially when the pyramid is in motion.

Figure 1. Proposed calibration frame assembled, with a scale bar (899.954 mm) inside it.

4. METHOD

4.1 Data collection

First the GCPs and CPs (in a local system) were determined in-air using a high-resolution SLR camera, namely a Nikon D750 SLR camera with a Nikon Zoom-Nikkor 24-70mm f/2.8 ED G AF-S Lens. Each image was captured with a fixed focus set and no alterations to the camera settings during data collection. The distance and height of the object were kept constant. For the data capture in air, a scale bar was placed together in the centre of the calibration frame. An example capture layout is provided in Figure 2 with the scale bar being highlighted in red. The calibration frame and image capture fulfilled all four criteria required for reliable calibration formerly mentioned.
For the underwater image capture, two cameras have been used: Canon G7X (Canon, 2014) and a GoPro HERO5 Black (GoPro, 2019) in Table 2. Both are low-cost cameras suitable for photogrammetric applications underwater. These are the cameras

which will be utilised for further research and therefore being the focus of this investigation. The GoPro 5 Black camera was operated in the linear mode.

	Canon G7X	GoPro 5 Black
Dimension (pixel)	5472x3648	4000x3000
F-Stop	f/4	f/2.8
Exposure time	1/500 sec	1/330 sec
ISO speed	ISO-125	ISO-100
True focal length	9mm	3mm
Sensor size (mm)	13.20 x 8.80	6.17 x 4.55

Table 2. Canon G7X and GoPro Hero 5 specifications

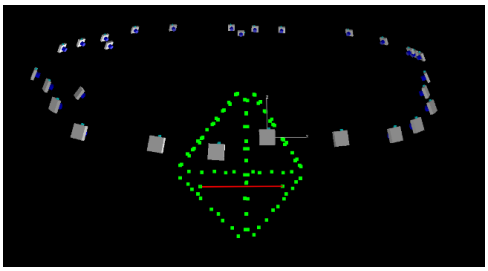

Figure 2. 3D view of camera locations during the data capture extracted from iWitnessPro. Green dots are the control points on the frame, the red bar is the scale bar used.

4.2 Data processing

Images were processed in commercial software, where a least-squares adjustment using the Brown camera model (Brown, 1971) was used to determine the values of the Interior Orientation Parameters (IOP) and Exterior Orientation Parameters (EOP), as well as the RMS of the GCPs after the adjustment and the coordinates of the CPs for an independent assessment of the accuracy. GCPs and CPs were observed in images using a centroid fitting method. The IOPs solved are: the principal distance (*c*) as the distance between the camera centre and the image plane, and the principal point offset (*xp, yp*) as the location of the principal point in the image plane. Furthermore, the following distortion parameters were used: radial lens distortion (*k1-k3* if not indicated otherwise), decentring distortion (*p1-p2*) and linear distortions (*b1-b2*). The adjustment was constraint by the dimension of the scale bar (899.954 mm).

4.3 Data analysis

The adjustments have been assessed using:

- Quality of Self-calibration (self-calibration score)
- Point referencing error.
- RMS of GCPs or control base lines
- RMS of CPs or check baselines
- Percentage error

The "Quality of Self-calibration" is calculated during the bundle adjustment procedure. "The Quality of Self Calibration has an optimal value of 1.0, and values to 1.5 are acceptable. Values higher than 1.5 indicate a weak network geometry and thus sub-optimal determination of camera parameters." (iWitness Manual, 2019). A good network geometry is critical for any Least Square Adjustment.

The RMS of the image point residuals (RMS Vxy), also called point referencing errors, is used as an indicator for the quality of the bundle adjustment. Assessing the RMS Vxy, allows to ascertain the likelihood of successfully orientating all images in the set to each other. A value less than 0.5 pixel in air and 1 pixel underwater is desired, and achievable considering the quality of the images, their overlap, and the high redundancy of the Least Squares Adjustment.

The Quality of Self-calibration (self-calibration score) and the Point referencing error, the RMS of GCPs or control base lines as well as the Percentage error, were used to assess the relative accuracy of the adjustment. The RMS values are outputted from the software for the GCPs and manually calculated for the CPs.

Where GCPs were calculated in an independent adjustment or if CPs were compared to a reference, the signed distances between the two datasets were calculated and tested for significance with a t-test. The same method was applied to assess using base lines. Where baselines were used, the baselines were split into two sets. One set was used to constrain the Least Squares Adjustment, while the other set was used for an independent accuracy assessment. This comparison was used to assess the absolute accuracy which could be achieved.

Three different tests were carried out:

1. *Reliability of the frame*: to check if the frame can be put together in such a way that the GCPs are unchanged. This was performed in-air only.
2. *Repeatability*: To see if the same results can be achieved for different photogrammetry software products, and using different cameras. This aspect is important for the practical use of the frame for further research. The test is only performed in-air, too.
3. Underwater performance test: The calibration frame is verified in an underwater setting as this is the intended application of the frame.

5. RESULT

The results of the different tests are presented below.

5.1 Reliability of the frame

To test the reliability of the frame, the capture of the in-air test was repeated on two different datasets captured during different days. Between the data captures the frame was dismantled and put away in the tubing simulating the field procedure. Both datasets were processed independently in a free adjustment. The only constraint introduced is the length of the scalebar. A total of 88 coordinate points were observed in each dataset and used in a free network Least Squares Adjustment utilising the iWitnessPro software.

The PRE and self-calibration score from the adjustments of the two datasets is presented in Table 3. The point referencing error for both datasets is below 0.5 pixels below the defined threshold. The self-calibration score is 1.1 for both datasets and below the threshold of 1.5. Hence, it is concluded that both adjustments have been successful.

	Dataset 1	Dataset 2
PRE	0.49 pixel	0.37 pixel
Self-calibration score	1.1	1.1

Table 3. Results of the LSA of dataset 1 and 2 using iWitness.

The derived 3D coordinates of the GCPs from both independent adjustments are used to calculate the residuals between the GCPs. Overall, 88 points could be utilised to calculate the residuals. The residuals are plotted in Figure 3, applying a uniform scale factor for on the residuals of 0.8335 mm to make any possible trends visible. The residual plot shows a bias towards the centre of the frame. This bias could be caused due to the frame not being able to be re-assembled tin exact the same manner.

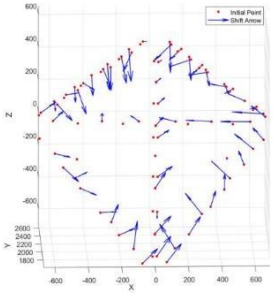

Figure 3. Residual (blue arrow) between the GCPs of dataset 1 (reference) and dataset 2. The residuals are scaled to make a possible trend visible.

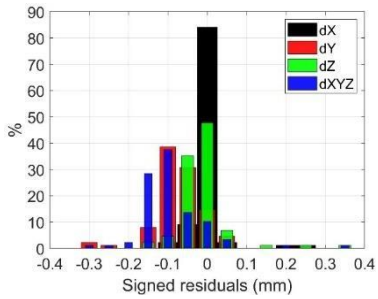

Figure 4. Residual plots of the X, Y, Z and overall residuals between the GCPs of dataset 1 and dataset 2.

The distribution of the signed residuals between the GCPs for the three axes and combined are presented in Figure 4. The detected bias is also visible here especially in the y coordinates of the GCPs.

The RMS of GCPs is presented in Table 4. Overall, RMS values were less than 2mm. Results of the t-test found that the residuals of the GCPs in X and Z are not significant. However, the Y value residuals show a significant difference which fits to the observations of Figure 3 and Figure 4.

RMS X dimension	0.4043mm
RMS Y dimension	1.0142mm
RMS Z dimension	1.1551mm
Overall RMS	1.5894mm

Table 4. GCP RMS of dataset 1 and 2 using iWitness.

Even though there are very small residuals, there is a systematic trend which could be caused by resembling the frame. Therefore, using the GCPs is assumed to be not sufficient. Instead, baselines will be used for any further processing.

5.2 Repeatability of results

Based on the results of the previous test, not GCPs but baselines were used to constraint the adjustment and to assess its processing results. On each of the six legs of the frame 2-3 baselines were defined (shown as red lines in Figure 5). As the baselines were all connected to a single leg of the pyramid, it is assumed that any bias from reassembling the frame can be removed. Overall, 14 baselines were introduced this way. Six of those baselines were kept fixed for the processing in the different software solutions. The remaining eight baselines were used for an independent accuracy assessment, to be validated if results achieved by different software products were comparable. The baselines extracted from dataset 1 was used as reference.

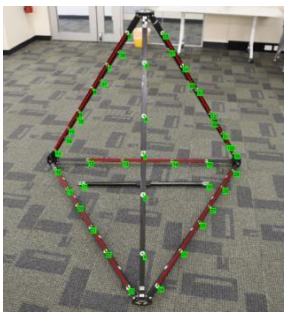

Figure 5. Baseline locations (red) on the frame derived y GCPS (green) on single parts of the frame.

Three software solutions were selected to process the Dataset 2 images. The software solutions were iWitness (version 4.105), Metashape (version 1.8.3) and ContextCapture (version 10.19.0.122). All adjustments using the Metashape software used the radial lens distortion parameters *k1-k4*. A summary showing all adjustment results is provided in Table 5. The adjustments were assessed to be successful, as the maximum point referencing error was 0.49 pixels, which was and under the defined threshold of 0.5 pixel. Furthermore, the maximum GCP RMS was 0.88 mm, which is within the defined range of 0.5 – 3 mm.

	iWitness Pro	Context-Capture	Metashape
PRE	0.49 pixel	0.37 pixel	0.49 pixel
RMS [mm]	0.88	0.74	0.78

Table 5. Results of the LSA of dataset 2 using iWitness, Metashape and ContextCapture.

It was not possible to observed the points belonging to check baselines in Metashape as part of the bundle adjustment. Hence, using Metashape only, a 3D model of the frame had to be created based on a dense point cloud derived from the processed images. The baseline points were then observed as a 3D model using CloudCompare, serving as the foundation for all measurements resulting from the Metashape software. However, the accuracy of performing such observations is heavily reliant on the human eye and the ability to pick the points manually in the 3D model, as well as the quality of the model itself. Next to the adjustment errors, additional error caused by the dense reconstruction, as well as the creation of the model will impact the observations.

A histogram showing the residuals of the extracted check baselines from Dataset 2, compared to the reference baselines from Dataset 1 processed with iWitnessPro is shown in Figure 6. the distribution of values in Figure 6, suggested a negative bias for the iWitnessPro software and a positive bias for ContextCapture software visible.

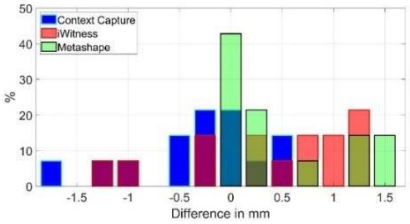

Figure 6. Residual plots of the different baselines distance depending on the software.

For a more detailed analysis, all baseline residuals were presented in Table 6. The RMS of the baseline residuals from all software solutions was within the acceptable magnitude of 3 mm, with values of 0.702 mm, 0.314 mm and 0.570 mm for the software iWintessPro, ContextCapture and Metashape, respectively. The average of the signed residuals shows a positive bias for Metashape (0.354 mm), a negative bias for ContextCapture (-0.132 mm) and no significant bias for iWitnessPro (0.019 mm). In contrast, the range of the residuals is the largest for the iWitness software.

To further investigate reliability, two additional cameras were added to the validation: the Canon G7X and the GoPro Hero5. By incorporating these different camera models, the aim was to assess the repeatability of the results across multiple devices, minimising any potential biases or limitations associated with a single camera. The additional cameras selected for the test were the same which will be used for Test 3 (underwater validation). For this test only the ContextCapture and Metashape software are used. The rationale was that these are the software solutions to be used in the next stage of the project.

Differences	iWitness-Pro	Context Capture	Meta-shape
Baseline 1	0.809	-0.038	0.123
Baseline 2	0.462	-0.344	0.111
Baseline 3	0.291	-0.325	0.132
Baseline 4	-0.945	0.344	0.169
Baseline 5	-1.204	-0.495	0.237
Baseline 6	0.702	0.066	1.350
RMS	0.795	0.314	0.570
Average	0.019	-0.132	0.354
Range	2.013	0.839	1.461

Table 6. Baseline residual and RMS of the dataset 2 processing results using iWitnessPro, Metashape and ContextCapture. All values are in [mm].

A summary showing all adjustment results for the three cameras for the ContextCapture and Metashape is provided in Table 7. The adjustments were assessed to be successful for the Canon G7 camera, as the maximum point referencing error is 0.56 pixels, which only just above the defined threshold of 0.5 pixel for in-air applications. The point referencing error of the Canon camera was identical for the two software used. The RMS value was also identical for both software for this camera with 1.31 mm, which was nearly double of the value for the Nikon D750 camera, but still below our defined threshold of 3 mm. The results for the percentage were comparable to the results from the RMS analysis. The results of the proceeding of the GoPro camera were borderline. The RMS values for both software were 1.47 mm and 1.57 mm, respectively, and below the defined threshold. However, the point referencing error was above the threshold, and were 0.63 mm and 0.83 mm for the ContextCapture and Metashape software, respectively. It is possible that the GoPro cameras were borderline due to using only *k1-k4* parameters to model the radial lens distortion, which may not be sufficient for the fisheye distorted images.

	ContextCapture			Metashape		
	Nikon D750	Canon G7X	Go-Pro	Nikon D750	Canon G7X	Go-Pro
PRE pixel	0.37	0.56	0.63	0.49	0.56	0.83
RMS [mm]	0.74	1.31	1.47	0.78	1.32	1.57

Table 7: Results of the LSA of dataset 2 using Metashape and ContextCapture in combination with three different cameras.

The RMS increased using the lower grad cameras, compared to the Nikon D750 SLR used for the previous tests, which reflects the results presented in Table 7. The negative bias of the ContextCapture software was visible for all cameras but significantly larger for the lower grade cameras (Table 8). In contrast, the positive bias of the Metashape software for the Nikon D750 SLR turns into a negative bias with by far the largest magnitude. The Metashape results could have been impacted by the method of how the check baseline observations were performed, as discussed previously. Overall, though, all RMS values were within the acceptable defined range of 0.5 – 3 mm.

Base-line	ContextCapture			Metashape		
	Nikon D750	Canon G7X	GoPro	Nikon D750	Canon G7X	GoPro
1	-0.04	-1.77	-0.91	0.12	-1.52	-1.28
2	-0.34	-1.08	-2.42	0.11	-1.41	1.46
3	-0.33	-1.10	0.67	0.13	-1.34	-1.49
4	0.34	0.89	-1.17	0.17	-1.32	-1.52
5	-0.50	-1.49	1.53	0.24	-1.24	-1.99
RMS	0.34	1.31	1.47	0.16	1.32	1.57
Avrg	-0.09	-0.54	-0.14	0.16	-0.91	-0.54
Range	0.84	3.08	3.95	0.13	2.89	3.56

Table 8. Baseline residuals [mm] and statistics of the dataset 2 processing results using Metashape and ContextCapture using three different cameras.

5.3 Underwater performance test

For the underwater performance test, the calibration frame was submerged in shallow and clear water, and images were captured using the previously tested Canon G7X (Figure 7) and the GoPro HERO5 Black (Figure 8). Images were captured on 29/5/2023 at Coogee Beach, Perth, Australia (S32.105569, E115.761822). The images were captured in the same manner as they were taken previously making them suitable for self-calibration.

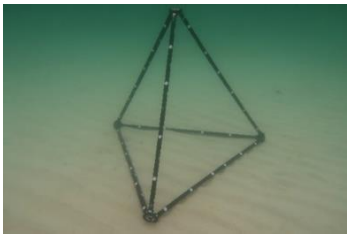

Figure 7. Proposed calibration frame underwater captured using the Canon G7X camera.

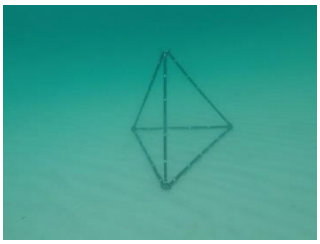

Figure 8. Proposed calibration frame underwater captured using the GoPro 5 Black camera.

Table 9, compares the performance of the two software programs: ContextCapture and Metashape, for the two different camera models: Canon and GoPro. In terms of point reference error in pixels, both ContextCapture and Metashape show higher values for the GoPro camera compared to the Canon camera. In ContextCapture, the point reference error was 0.91 pixels for the Canon camera and 1.39 pixels for the GoPro camera. In Metashape, the point reference error was higher for both, with values of 2.82 pixels for Canon and 3.6 pixels for GoPro. Considering the defined threshold of 1 pixel, only the Canon software processing the data with the ContexCapture software (0.91 pixel) passed the defined threshold requirements. The GoPro camera using the ContextCapture software was just above the threshold of 1 pixel with a value of 1.39 pixel. It can be concluded that the ContextCapture software was suitable to produce the required accuracy.

In terms of RMS error in mm, the Canon camera again performed better than the GoPro, but although ContextCapture again performed better than Metashape, the values were similar camera models. For the Canon, ContextCapture, the RMS error was 1.02 mm and in Metashape it was 1.32 mm; and for the GoPro, ContextCapture had an RMS of 1.90 mm and Metashape was 1.96 mm. Importantly, all values were within the threshold of 3 mm.

The RMS values for the check baseline residuals from the underwater test (Table 10), were generally slightly higher, compared to the in-air test (Table 8); however, still below the desired maximum threshold of 3 mm. In the ContextCapture software, the RMS value increased from 1.31 mm and 1.47 mm in air, to 1.63 mm and 1.90 mm underwater for the Canon and GoPro camera, respectively. The Metashape software again had larger values. For the Metashape software, the RMS value increased from 1.37 mm and 1.57 mm in air, to 1.80 mm and 1.96 mm underwater for the Canon and GoPro camera, respectively.

	ContextCapture		Metashape	
	Canon G7X	GoPro	Canon G7X	GoPro
PRE pixel	0.91	1.39	2.82	3.63
RMS [mm]	1.02	1.90	1.32	1.96

Table 9: Results of the LSA of the underwater dataset using Metashape and ContextCapture in combination with two different cameras.

Differences (mm)	ContextCapture		Metashape	
	Canon G7X	GoPro	Canon G7X	GoPro
Baseline 1	0.92	-2.28	-1.38	2.00
Baseline 2	-1.01	1.46	1.35	-2.75
Baseline 3	1.03	-1.49	-1.36	1.25
Baseline 4	1.13	2.12	-1.35	-2.14
Baseline 5	-1.02	-1.99	-1.24	1.25
RMS	1.02	1.90	-1.32	1.96
Average	0.21	-0.44	-0.80	-0.08
Range	2.15	4.40	2.73	4.75

Table 10. Underwater baseline residual and RMS of the dataset 2 processing results using ContextCapture and Metashape.

6. CONCLUSION

The accuracy achieved by the various calibrations carried out using the proposed calibration frame, with different cameras and software combinations, demonstrated that the proposed calibration frame is an effective tool for achieving reliable camera calibration both in air and in water. The results were comparable, or better, than similar studies, particularly when baselines were used (Table 11).

In air camera performance tests, this study found that the Nikon D750 consistently achieved the lowest RMS values with both ContextCapture (0.74 mm) and Metashape (0.78 mm), indicating superior accuracy and imaging quality compared to the other cameras. While the Canon G7X generally performed better than the GoPro in both software environments.

In water tests, the study found the Canon G7X outperformed the GoPro in both software environments. Capra et al. (2015) also achieved better results with a compact Canon camera over a GoPro (Table 11). Results were similar between software used. With ContextCapture, the Canon G7X achieved a lower RMS value of 1.02 mm, while the GoPro scored 1.90 mm. Similarly, using Metashape, the Canon G7X obtained an RMS value of 1.32 mm, and the GoPro scored 1.96 mm. Canon performance better than the GoPro, which is likely due to the better camera sensor and specifications (e.g. sensor and image size). This study achieved better results using Context Capture than MetaShape. Nevertheless, overall, it can be concluded that the results are acceptable for both cameras and software solutions.

Study	RMS (mm)	
	In-Air	In-water
Gourgoulis et al. (2008)	3.7 – 4.66	4.5-5.92
Challis and Kerwin (1992)	0.8	N/A
Helmholz et al. (2016)	N/A	0.45 – 2.5
Li et al. (1997)	N/A	10.83
Capra et al. (2015)	N/A	-Hero2: 43.03 mm -Intova Sport HD: 11.330 mm -Canon PowerShot G12: 0.524 mm
This study	ContextCapture: Nikon D750: 0.74 Canon G7X: 1.31 GoPro: 1.47 Metashape: Nikon D750: 0.78 Canon G7X: 1.32 GoPro: 1.57	ContextCapture: Canon G7X: 1.02 GoPro: 1.90 Metashape: Canon G7X: 1.32 GoPro: 1.96

Table 11. Comparison of calibration results from selected studies compared to the current study.

ACKNOWLEDGEMENTS

The authors would like to thank King Abdulaziz University for funding Alaa Mufti's PhD study. We also express our thanks to Mr Malcolm Perry and Mr Luke Mickan from Curtin University for supporting to build the frame. Furthermore, we would like to acknowledge Curtin's 3D Hub and HIVE to utilise their facilities for the data processing and visualisation.

REFERENCES

Bouguet., 2017. Camera calibration toolbox for MATLAB. *California Institute of Technology*. http://www.vision.caltech.edu/bouguetj/calib_doc/index.html.

Brown., 1971. Close range camera calibration. *Photogramm Eng*, 37(8), 855–866.

Canon., 2014. Canon PowerShot G7X Mark II. Tokyo, Japan.

Capra, A., Dubbini, M., Bertacchini, E., Castagnetti, C., & Mancini, F,. 2015. 3D reconstruction of an underwater archaelogical site: Comparison between low cost cameras. *The International Archives of the Photogrammetry, Remote Sensing and Spatial Information Sciences*, 40, 67-72.

Challis, J. H., & Kerwin, D. G,. 1992. Accuracy assessment and control point configuration when using the DLT for photogrammetry. *Journal of Biomechanics*, 25(9), 1053-1058.

Diamanti, E., Spondylis, E., Vlachaki, F., & Kolyva, E,. 2017. Surveying the underwater arcaheological site of cape glaros at pagasetikos gulf. *The International Archives of the Photogrammetry, Remote Sensing and Spatial Information Sciences*, 42, 243-250.

Fraser, C. S., Shortis, M. R., & Ganci, G,. 1995. Multisensor system self-calibration. *Paper presented at the Videometrics IV*.

GoPro,. (2019). GoPro Hero 8 Black. GoPro, Inc, San Mateo, CA.

Gourgoulis, V., Aggeloussis, N., Kasimatis, P., Vezos, N., Boli, A., & Mavromatis, G,. 2008. Reconstruction accuracy in underwater three-dimensional kinematic analysis. *Journal of Science and Medicine in Sport*, 11(2), 90-95.

Guo, T., Capra, A., Troyer, M., Grün, A., Brooks, A. J., Hench, J. L., Schmitt, R. J., Holbrook, S. J., & Dubbini, M,. 2016. Accuracy assessment of underwater photogrammetric three dimensional modelling for coral reefs. *International Archives of the Photogrammetry, Remote Sensing and Spatial Information Sciences*, 41(B5), 821-828.

Harvey, E., & Shortis, M,. 1995. A system for stereo-video measurement of sub-tidal organisms. *Marine Technology Society Journal*, 29(4), 10-22.

Helmholz, P., Long, J., Munsie, T., & Belton, D,. 2016. Accuracy Assessment Of Go Pro HERO 3 (Black) Camera In Underwater Environment. *International Archives of the Photogrammetry, Remote Sensing & Spatial Information Sciences*, 41.

Jalal, A., Salman, A., Mian, A., Shortis, M., & Shafait, F,. 2020. Fish detection and species classification in underwater environments using deep learning with temporal information. *Ecological Informatics*, 57, 101088.

Li, R., Li, H., Zou, W., Smith, R. G., & Curran, T. A,. 1997. Quantitative photogrammetric analysis of digital underwater video imagery. *IEEE Journal of Oceanic Engineering*, 22(2), 364-375.

Samboko, H. T., Schurer, S., Savenije, H. H., Makurira, H., Banda, K., & Winsemius, H,. 2022. Evaluating low-cost topographic surveys for computations of conveyance. *Geoscientific Instrumentation, Methods and Data Systems*, 11(1), 1-23.

Shortis, M. (2019). Camera calibration techniques for accurate measurement underwater. 3D recording and interpretation for maritime archaeology, 11-27.

Shortis, M., Abdo, E. H., & Dave,. 2016. A review of underwater stereo-image measurement for marine biology and ecology applications. Oceanography and marine biology, 269-304.

Shortis, M. R., Clarke, T. A., & Robson, S,. 1995. Practical testing of the precision and accuracy of target image centering algorithms. Paper presented at the Videometrics IV.

Shortis, M. R., & Harvey, E. S,. 1998. Design and calibration of an underwater stereo-video system for the monitoring of marine fauna populations. International Archives of Photogrammetry and Remote Sensing, 32, 792-799.

Shortis, M. R., Miller, S., Harvey, E., & Robson, S,. 2000. An analysis of the calibration stability and measurement accuracy of an underwater stereo-video system used for shellfish surveys. Geomatics Research Australasia, 1-24.

Shortis, M. R., & Seager, J. W,. 2014. A practical target recognition system for close range photogrammetry. The Photogrammetric Record, 29(147), 337-355.

Wehkamp, M., & Fischer, P,. 2014. A practical guide to the use of consumer-level digital still cameras for precise stereogrammetric in situ assessments in aquatic environments. *Underwater technology*, 32(2), 111-128.

Yuan, S., Li, Y., Bao, F., Xu, H., Yang, Y., Yan, Q., Zhong, S., Yin, H., Xu, J., & Huang, Z,. 2022. Marine environmental monitoring with unmanned vehicle platforms: Present applications and future prospects. *Science of The Total Environment*, 159741.

Zhang, Z,. 2000. A flexible new technique for camera calibration. *IEEE Transactions on pattern analysis and machine intelligence*, 22(11), 1330-1334.

Chapter 3 - An Open-Source, Data-Logging Device for Marine-Based Surveys

This study introduces a low-cost, open-source device for accurate georeferencing in underwater photogrammetry, addressing seafloor mapping challenges. The system, featuring position and laser sensors, achieves high accuracy using the Post Processed Kinematic (PPK) technique. Echosounder measurements align well with lidar and RTK Rover data. The laser distance measurer, showing a correlation with the echosounder, demonstrates the effectiveness of low-cost platforms like Raspberry Pi for marine research. Future research aims to integrate this data into photogrammetry surveys.

Method	**Underwater Photogrammetry**		**Hydroacoustic**	
Disadvantages	Low positional certainty	Camera calibration required	No photomosaic	High resolution requires mutlibeam which is expensive and resource heavy
Advantages	Photomosaic	High resolution	High positional certainty	Reliable Bathymetry

Chapter 3: **An open-source, data logging device for marine-based surveys**
Aim: to create a device and platform for acquiring high accuracy positioning and bathymetry data for underwater photogrammetry surveys.

Mufti, A., Parnum, I., Belton, D., & Helmholz, P.: An Open-Source, Data-Logging Device for Marine-Based Surveys, *Int. Arch. Photogramm. Remote Sens. Spatial Inf. Sci.*, XLVIII-1/W2-2023, 1943–1948, https://doi.org/10.5194/isprs-archives-XLVIII-1-W2-2023-1943-2023, 2023

AN OPEN-SOURCE, DATA-LOGGING DEVICE FOR MARINE-BASED SURVEYS

A. Mufti[1,2]*, I. Parnum [1], D. Belton [1], P. Helmholz [1]

[1] School of Earth and Planetary Sciences, Curtin University
GPO Box U1987, Perth WA 6845, Australia, alaa.mufti@postgrad.curtin.edu.au, (Petra.Helmholz, I.Parnum, D.Belton)@curtin.edu.au
[2] King Abdulaziz University, Jeddah 21442, Saudi Arabia

Commission II WG II/7

KEYWORDS: Data logging, Open-source, Portability, Marine surveys,

ABSTRACT:

Observation, monitoring, and understanding of the marine environment, particularly seafloor mapping, have gained global attention. Underwater photogrammetry is a valuable technique for creating accurate seafloor orthomosaics and digital elevation models (DEMs). However, achieving accurate georeferencing in photogrammetry surveys is challenging in marine environments. To address this, a low-cost and open-source data collection device was developed for underwater photogrammetry projects. The device is affordable, flexible, lightweight, and capable of logging position, motion, and utilizing a laser for seafloor feature identification. This paper presents the validation and assessment of the system, focusing on the performance of the position and laser sensors. The study advances underwater photogrammetry and provides insights into the device's capabilities for marine research and mapping applications. The results show that the Post Processed Kinematic (PPK) technique achieves high accuracy, with RMSE values of 0.294 m (distance), 0.267 m (X-coordinate), and 0.12 3m (Y-coordinate) at the Fremantle car park and 0.278 m (distance), 0.16 8m (X-coordinate), and 0.222 m (Y-coordinate) at the Fremantle near boat ramp. PPP exhibits acceptable accuracy, while GPS shows relatively lower accuracy. Echosounder measurements correlate well with bathymetric lidar and RTK Rover reference data, with RMSE values of 45 cm and 28 cm, respectively. The laser distance measurer provides accurate measurements between 25 and 60 cm, showing a good correlation with the echosounder (R = 0.77). After correction for offset and refraction, the laser measurements have an RMSE of 1.8 cm compared to the echosounder. This study further demonstrated the feasibility and effectiveness of low-cost and open-source platforms, like Raspberry Pi, for marine research and mapping applications. Further work will investigate integrating this data into photogrammetry surveys.

1. INTRODUCTION

Observation, monitoring, and understanding of the marine environment, particularly seafloor mapping, are central topics of marine research that have received worldwide attention recently (Yuan et al., 2022). Underwater photogrammetry has been shown to be an effective method for creating orthomosaics and digital elevation models (DEMs) of the seafloor (Urbina-Barreto et al., 2021). To be able to create accurately georeferenced mosaics and DEMs, photogrammetry surveys require images to be tagged with position and motion data, and a number of Ground Control Points (James, Robson, & Smith, 2017); however, collecting data in the marine environment is technically and economically challenging.

Accurate data collection in the marine environment is crucial for better understanding and quantification of the seafloor (Yuan *et al.*, 2022). However, several challenges hinder the acquisition of reliable seafloor maps, including limited existing data and difficulties in data collection. These challenges arise from various factors, such as the remoteness and hazards that make it unsafe for ships to survey shallow areas (Iscar & Johnson- Roberson, 2015). Alternative systems like Autonomous Surface Vehicles (ASVs) or Remote Operation Vehicles (ROVs) offer safer options for data collection, but these systems can be expensive, time-consuming, and require specialized expertise to use effectively (Suhari, Karim, Gunawan, & Purwanto, 2017). This study's aim was to develop a low-cost, open-source, data collection device to support underwater photogrammetry projects, with the following criteria:

- Low cost.
- Open source, to allow flexibility.
- Lightweight so that it could be operated by a snorkeller, swimmer, kayaker or an Autonomous Surface Vessel (ASV).
- Simultaneously log position (X, Y, Z) – both depth down from the water surface and altitude above the seafloor, and motion (heading, pitch and roll). That could be tagged to images collected.[1]
- A laser to identify the location of features in imagery on the seafloor.

This paper presents the validation and assessment of the system, particularly the performance of the position, the echosounder, and laser sensors. The paper is structured as follows an

* Corresponding author

introduction section that sets the context and outlines the objectives, followed by a comprehensive literature review to establish the theoretical background. The next section provides a detailed description of the system, highlighting its key features. The validation and assessment process are then presented, discussing the methodology, experimental setup, and obtained results. Finally, the paper concludes with a summary of the key insights, implications of the study, and suggestions for future research directions.

2. RELATED WORKS

While there are several examples of commercial devices capable of simultaneously collecting data for depth and position, some of these were either too expensive and/or not adaptable enough to meet all the needs for the current study. For instance, Suhari *et al.* (2018) developed small ROV boats equipped with remote sensing technology, GNSS, echo sounder, and navigational engine for bathymetry surveys in Malaysia. However, both platforms could not be adapted to meet the study's criteria. However, there were examples of open-source platforms developed for similar applications. Gogendeau (2022), who created an open-source ASV solution for tracking slow-moving marine animals. It uses a short baseline (SBL) acoustic system with a 100 m range. The ASV also collects environmental data and is designed to be low-cost and adaptable for adding other sensors.

Karegar *et al.* (2022) designed a unit to measure water levels, the Raspberry Pi Reflector (RPR) prototype incorporates a low-cost, low-maintenance GPS module and navigation antenna connected to a Raspberry Pi microcomputer. Operating successfully since March 2020 near the Rhine River in Wesel, Germany, it retrieves sub-daily and daily water levels through spectral analysis of reflection data.

Thapliyal & Kumar (2016) have designed a unit to monitor critical parameters and motion detection in restricted compartments onboard, the integrated proof of concept Data Acquisition Console (DAC) prototype utilizes various sensors interfaced with a Raspberry Pi board. The objectives of the study by Thapliyal & Kumar (2016) the project, includes: real-time monitoring of temperature, humidity, and access to restricted compartments, remote access through a web-based site on the ship's LAN, data logging for analysis, and the addition of a pressure sensor for validation and altitude calculation.

Wootton (2020) designed an ASV for marine magnetic and bathymetric surveying. Equipped with Raspberry Pi 2 and Raspberry Pi 3B+ modules, along with a single frequency echo sounder and a magnetometer, the ASV collected data. A Python script synchronized bathymetric and GPS location data, creating a central data collection system. This system received data from the magnetometer, echo sounder, and single point positioning system, resulting in a synchronized geospatial dataset stored within the Raspberry Pi. The survey vessel configuration underwent testing in three Canadian lakes.

Guo & Bräunl (2020) designed a unit using Raspberry Pi 3B for measuring and logging key parameters. The system logs water temperature, pressure, battery level, current speed, GPS coordinates, pitch, yaw, and roll. Data transmission allows communication between various sensors. Additionally, a telemetry method enables remote data storage in a database, real-time monitoring of position and key parameters, and an IoT application for LAN communication and data display on dashboards accessible by multiple devices.

In conclusion, this study explored various examples of commercial and open-source devices for data collection in-depth and position-related applications. The evaluation revealed that while some commercial devices were expensive or lacked adaptability, open-source platforms provided promising solutions. Notable examples included platforms for georeferenced underwater photogrammetric mapping and an autonomous surface vessel (ASV) for marine tracking. Hence, this study was inspired by these related works to be based on an open-source devices. Based on the available options at the time, the Raspberry Pi was determined to be the most suitable device for the study's objectives. Several studies highlighted the successful integration of Raspberry Pi with various sensors for measuring water levels, monitoring critical parameters, controlling environmental factors, and conducting marine surveys. These examples provided valuable insights and inspiration for the current study, showcasing the versatility and cost-effectiveness of open-source devices in data collection applications.

3. PROPOSED DEVICE

A schematic diagram, and a photo of the data logging device, are shown in Figures 1 and 2, respectively. A list of the main components and their cost is detailed in Table 1. The data logging device was built around a Raspberry Pi, as these are low-cost, low-power consumption, small-sized computer with open-source software and a Python application for controlling, collecting, and storing sensor data simultaneously. The open-source nature of Raspberry Pi, which enables the development of study-specific analysis, is a key advantage (Addona et al., 2022).

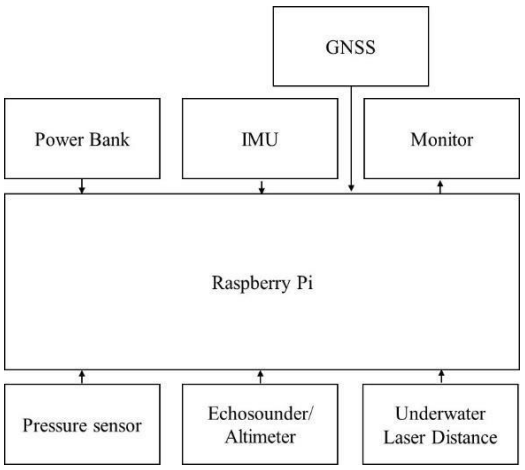

Figure 1. A schematic of the data logging device and the sensors integrated.

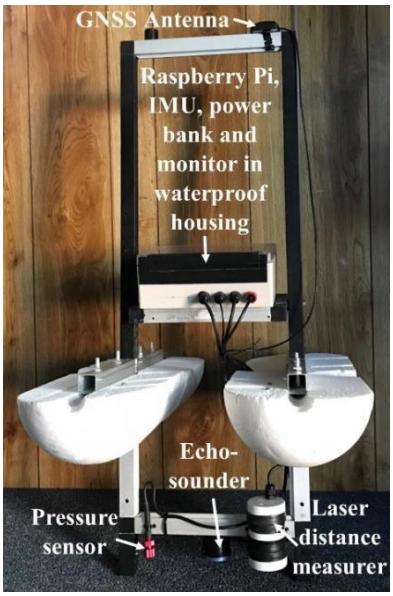

Figure 2. Photo of the data logging device and sensors mounted on a frame.

Component	Role	Price (US$)
Raspberry Pi 4	The Raspberry Pi 4 is the main unit that collects and saves the data.	123
Pressure Sensor	Used for measuring the depth down from the sea surface. Accuracy is 2 mm.	85
GNSS Antenna	Used to find the location of the vehicle. RTK compatible.	42
Echosounder/ Altimeter	Uses sound to get the altitude from the seafloor to the sensor. Resolution is 0.5% of range.	312
IMU	An Inertial Measurement Unit (IMU) chip to measure motion. Including gyroscope and accelerometer.	53
Laser distance measurer	Uses green light to get the altitude from the seafloor to the sensor. Accuracy is +/- 3mm.	70
Power bank	To supply the power to the Raspberry Pi and Monitor.	54
Monitor	Used to show the data from the Raspberry Pi 4	79
Styrene floats	Used to keep the vehicle floating on the sea surface	2 X 35
Total cost		US$ 888

Table 1. Components used in the data logging device and their cost (US$).

Integrated into the Raspberry Pi were a RTK compatible GNSS (the SparkFun GPS-RTK Board - NEO-M8P-2 Receiver), an echo-sounder/altimeter (Blue Robotics Ping Sonar), a pressure sensor (Blue Robotics Bar30), a green laser distance measurer (JRT), and a monitor (Figure 1 and Figure 2, Table 1). This was all powered by a 2600mA power bank, which was able to power it for at least 3 hours (Figure 1). The Raspberry Pi, IMU, and power bank were enclosed in a waterproof housing. The waterproof housing was attached in the middle of a rectangle rigid, metal frame. The GNSS antenna was attached to the top of the frame and positioning directly above the echosounder and laser distance measurer, with the pressure sensor located adjacent, attached to the bottom of the frame (Figure 2). Styrene floats were added for floatation and to provide a stable platform (Figure 2). A program was written in Python to log the sensor data and time stamp with the GNSS every second.

4. VALIDATION

Tests were carried out to assess the accuracy of the device's:

1) Positioning solution provided by the GNSS receiver both in real-time and post-processed.
2) Depth measurements using the echosounder.
3) Depth measurements of the laser distance measurer.

4.1 Datasets

To assess the positioning solution of the GNSS receiver, in-air data collection was conducted twice at Fremantle Sailing Club in Perth, Western Australia. The first test was in the car park (S-32.07033961, E115.7496281 WGS 84) and the second test was near the boat ramp (S-32.07014067, E115.750357 WGS 84). To assess the accuracy of the GNSS receiver and the Post Processed Kinematic (PPK) and Precise Point Positioning (PPP) solutions, the main objective of this study was to compare their position solutions with a Trimble RTK Rover survey that collected discrete points. Two techniques, namely Post Processed Kinematic (PPK) and Precise Point Positioning (PPP), were employed to refine the accuracy of the raw GPS data through error correction and improved positioning results. This study provides valuable insights into the performance of GNSS positioning techniques in real-world scenarios, demonstrating the accuracy, reliability, and effectiveness of raw GPS, PPP and PPK. The comparison with the reference RTK data facilitated the determination of the superior method based on the evaluation of Root-Mean-Squared Error (RMSE) values.

To assess the depth measurements from the echosounder and laser distance measurer, data was collected with the device over a boat ramp at Fremantle Sailing Club, Western Australia (Figure 3, Figure 4, and Figure 5). Echosounder data collected with the Raspberry Pi were corrected for physical offsets, sound velocity and measured tide from Fremantle Fishing Harbour, then converted to Australian Height Datum (AHD) using the Australian Coastal Vertical Datum Transformation Tool (CRCSI, 2016). This data was compared with historic bathymetry LiDAR data (Fugro, 2009), and a Trimble RTK Rover survey that collected discrete points over the boat ramp area, which were both re AHD (Figure 4), to enable a comparison over all of the survey area. As the historic bathymetric lidar data was gridded at 5 m (with a projection of MGA Zone 50), data from the echosounder and RTK Rover surveys were (mean) gridded to the same grid nodes as the bathymetric lidar data, where data was present, to allow a direct comparison. Gridded data were compared by calculating Pearson's correlation coefficient, least-

means-squared linear regression and root-mean squared error (RMSE).

The laser distance measurer was an off-the-shelf in-air sensor that was sealed in an underwater housing. The green light produced by the laser can be seen over an underwater target placed in the harbour in Figure 5. As the measurements outputted by the device assume it is in-air, the water index was calculated as per standard formulations (IAPWS, 1997), to correct the distances logged for change in the speed of light. The laser distance measurer was compared with the echosounder data using Pearson's correlation coefficient and least-means-squared linear regression. The intercept (c) of the linear regression (y = mx +c), was used to establish the: fixed height offset between the acoustic centre of the echosounder and the optical centre of the laser distance measurer. The slope (m) of the linear regression was compared to the water index of (green) light (m) as an empirical estimate of the effect of refraction. The distances outputted by the laser were corrected for the height offset and water index and were then filtered using +/- 10% of the echosounder depth for the same measurement. The RMSE was calculated between the corrected laser and the echosounder measurements.

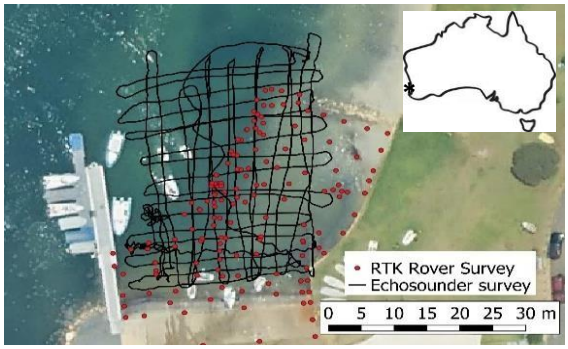

Figure 3. Data collection in Fremantle Sailing Club (FSC): (top) the track of device collecting echosounder data as a black line, the Trimble R12 Rover positions as red circles, over an aerial photograph, and location of FSC (*) in Australia (insert).

Figure 4. the Trimble R12 Rover data being collected.

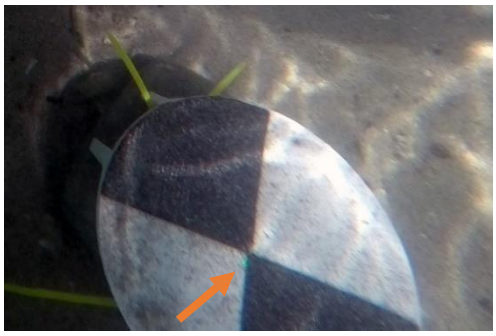

Figure 5. Green laser (arrow) on an underwater target.

4.2 Evaluation of GNSS

The tracks of the GNSS validation test of GPS, PPP, and PPK techniques in the FSC car park area are shown in Figure 4. It can be seen in Figure 6, and the resulting RMSE values in Table 2, that PPK was the closest of the three positioning solutions to the RTK data. For instance, PPK had the lowest RMSE values in all three categories: distance of 0.294 m, X-coordinate of 0.267 m, and Y-coordinate of 0.123 m. GPS exhibits relatively higher RMSE values, with distances of 2.740 m, X-coordinate of 1.927 m, and Y-coordinate of 1.948 m. PPP shows higher RMSE values compared to PPK, with distances of 2.068 m, X-coordinate of 1.806 meters, and Y-coordinate of 1.007 m. A similar result was found for the boat ramp test, as seen in the track plot in Figure 7, and the RMSE values in Table 3. Where PPK again had the lowest RMSE values in comparison to RTK, in the distance, X and Y directions. Again, GPS and PPP exhibited higher RMSE values in all three categories (Table 3).

In conclusion, the GNSS validation test comparing the GPS, PPP, and PPK techniques in the Fremantle car park area and boat ramp area revealed distinct performance variations. The results demonstrated that PPK was the closest to the reference RTK data, with the lowest overall error. In contrast, GPS and PPP exhibited higher levels of error in all three categories. These results are constant with other studies and confirm PPK as the best solution available for this system.

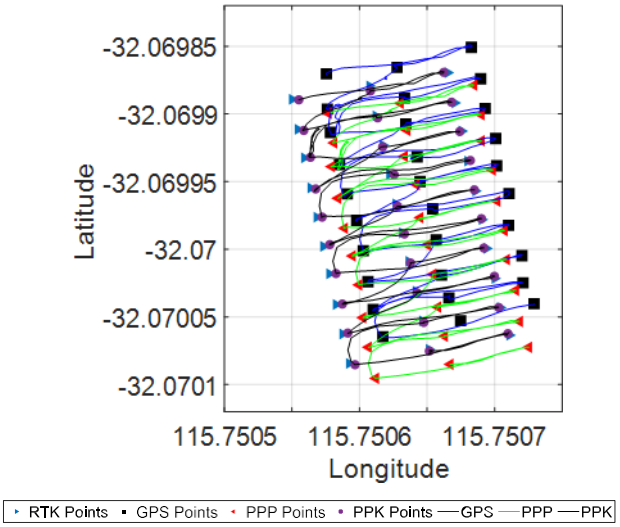

Figure 6. Position data results for GPS, PPK and PPP compared with RTK in Fremantle Car Park.

RMSE (m)	GPS	PPP	PPK
Distance	2.740	2.068	0.294
X	1.927	1.806	0.267
Y	1.948	1.007	0.123

Table 2. Position data results for GPS, PPK and PPP compared with RTK RMS

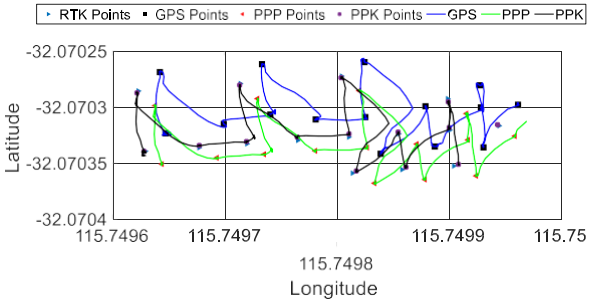

Figure 7. Position data (collected in-air) results for GPS, PPK and PPP compared with RTK in Fremantle near boat ramp.

RMSE (m)	GPS	PPP	PPK
Distance	2.971	1.954	0.278
X	2.094	1.582	0.168
Y	2.108	1.147	0.222

Table 3. Position data (collected in-air) results for GPS, PPK and PPP compared with RTK RMS.

4.3 Evaluation of the echosounder

Depth derived from the echosounder logged by the low-cost device, is compared against bathymetric lidar data, and the RTK Rover survey, in Figure 8. The echosounder data were highly correlated with both the LiDAR data (R = 0.92) and RTK survey (R = 0.89) (Table 3). Linear regression analysis showed the echosounder data had a similar rate of change to the reference data, but slightly deeper depths (12 and 34 cm). The echosounder data had an RMSE of 45 cm with the lidar data, and 28 cm with the RTK Rover survey (Table 4).

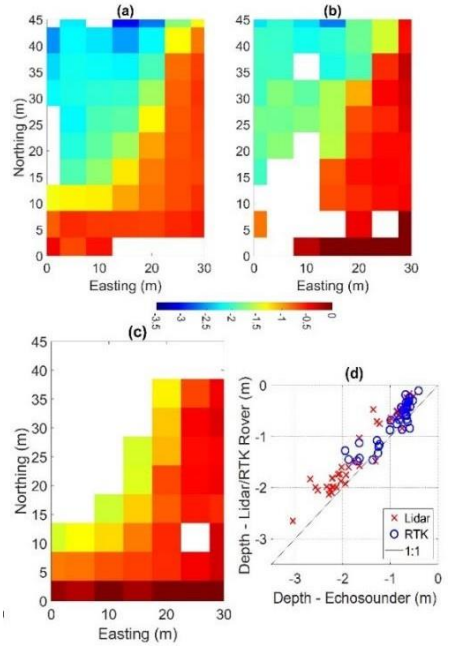

Figure 8. Depth data (re AHD) from Fremantle Sailing Club boat ramp: (a) gridded data from echosounder collected using the low-cost device; (b) gridded historic bathymetric LiDAR; (c) gridded RTK Rover survey; and (d) a Cartesian plot comparing depth data.

Reference data	Pearson's correlation coefficient	Linear regression coefficients	RMS (m)
Bathymetric lidar	0.92	y = 1x + 0.34	0.45
RTK Rover	0.89	y = 0.91x + 0.12	0.28

Table 4. Comparison of the Echosounder data with bathymetric lidar and RTK Rover reference data.

The echosounder results were comparable to the LiDAR and RTK measurements. The small differences between the depth measurements from the different platforms appear to be a constant error (12-34 cm), such as possibly from inadequate physical offset correction or the datum transformation from LAT to AHD, rather than a variable error.

4.4 Evaluation of the laser distance measurer

The laser distance measurer collected measurements between 25 and 60 cm Figure 9. Beyond 60 cm, the light was sometimes still visible but reliable measurements were not returned. Typically, lighter (close to white) surfaces appeared to be the most reliable for seeing the green light. The measurements between 25 and 60 cm correlated well with the echosounder (R = 0.77). The water index was calculated: theoretically as 1.34, and from the slope of the regression as 1.32. The laser distance measurements corrected for the physical offset and refraction, and filtered, had a RMSE of 1.8 cm with the equivalent echosounder measurements.

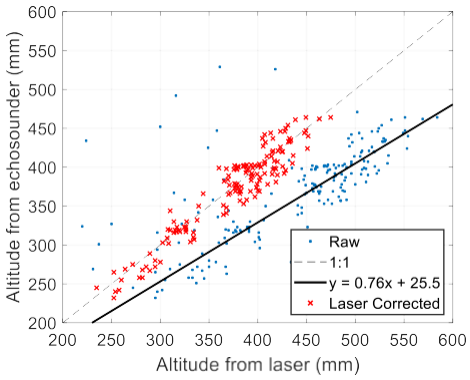

Figure 9. Altitude recorded by the laser vs echosounder: showing raw values from both devices (blue dots), and corrected laser distance values (red crosses). The black dashed line is the 1:1 ratio, and the solid black line is the best fit result from linear regression on the raw values.

The laser distance measurer during this study provided raw measurements, between 25 and 60 cm, that correlated well with the echosounder measurements. Laser measurements from longer distances might be possible, through using targets that are more optically reflective, and/or increasing the output power of laser. Nevertheless, having the laser visible on simultaneously acquired images, without a reliable distance measurement, still might be useful in locating the position of targets. However, effects of refraction would need to be adequately accounted. This study found that the effects of refraction could be corrected using either a theoretical or empirically derived index of water.

5 CONCLUSION AND FURTHER WORK

This study presented a low-cost and open-source data collection device designed to address the challenges of accurate georeferencing in underwater photogrammetry surveys. The device successfully collected accurate X, Y, Z positions, providing valuable data for photogrammetry work. The results showed that the Post Processed Kinematic (PPK) technique achieved the highest accuracy, while the Precise Point Positioning (PPP) technique exhibited acceptable accuracy. The Global Positioning System (GPS) showed relatively lower accuracy. Additionally, the device incorporated a laser for seafloor feature identification, which proved to be effective within a range of 25 to 60 cm.

This study further demonstrated the feasibility and effectiveness of low-cost and open-source platforms, like Raspberry Pi, for marine research and mapping applications. In addition, it provided an assessment of the sensor's capabilities and performance. Further work will investigate integrating this data into photogrammetry surveys.

ACKNOWLEDGMENT

The authors would like to thank King Abdulaziz University for funding Alaa Mufti's PhD study, and Mr Malcolm Perry and Mr Ming Lim from Curtin University for technical support.

REFERENCES

CRCSI,. 2016. AusCoastVDT version 1.20 User Manual. 27.

Fugro,. 2009. Western Australia Two Rocks to Cape Naturaliste Bathymetry and Seabed Survey LiDAR April/May 2009: Report of Survey. 168pp.

Gogendeau, P,. 2022. A Smart multi-sensor system for marine animals with embedded geolocation. *Université de Montpellier.*

Guo, J., & Bräunl, T,. 2020. Elfoil Data Logging, Transmission and Visualisation.

Iscar, E., & Johnson-Roberson, M,. 2015. Autonomous surface vehicle 3D seafloor reconstruction from monocular images and sonar data. *Paper presented at the OCEANS 2015-MTS/IEEE Washington.*

James, M. R., Robson, S., & Smith, M. W,. 2017. 3-D uncertainty-based topographic change detection with structure-from-motion photogrammetry: precision maps for ground control and directly georeferenced surveys. *Earth Surface Processes and Landforms, 42*(12), 1769-1788.

Karegar, M. A., Kusche, J., Geremia-Nievinski, F., & Larson, K. M,. 2022. Raspberry Pi Reflector (RPR): A Low-Cost Water-Level Monitoring System Based on GNSS Interferometric Reflectometry. *Water Resources Research,* 58(12), e2021WR031713.

Suhari, K. T., Karim, H., Gunawan, P. H., & Purwanto, H,. 2017. Small rov marine boat for bathymetry surveys of shallow waters–potential implementation in malaysia. *The International Archives of the Photogrammetry, Remote Sensing and Spatial Information Sciences,* 42, 201-208.

Thapliyal, A., & Kumar, C,. 2016. Development of data acquisition console and web server using Raspberry Pi for marine platforms. *International Journal of Information Technology and Computer Science,* 8, 46-53.

IAPWS,. 1997 http://www.iapws.org

Urbina-Barreto, I., Garnier, R., Elise, S., Pinel, R., Dumas, P., Mahamadaly, V., Facon, M., Bureau, S., Peignon, C., & Quod, J.-P,. 2021. Which method for which purpose? A comparison of line intercept transect and underwater photogrammetry methods for coral reef surveys. *Frontiers in Marine Science,* 8, 636902.

Wootton, M. R,. 2020. Autonomous Bathymetric and Magnetic Surveying for Canadian Lakes (Doctoral dissertation, Queen's University (Canada)).

Yuan, S., Li, Y., Bao, F., Xu, H., Yang, Y., Yan, Q., Zhong, S., Yin, H., Xu, J., & Huang, Z,. 2022. Marine environmental monitoring with unmanned vehicle platforms: Present applications and future prospects. *Science of The Total Environment*, 159741.

Chapter 4 - A novel platform and workflow for underwater photogrammetry surveys

This study leverages underwater photogrammetry to enhance marine mapping and habitat assessment for effective environmental management. Integrating sensors such as GNSS, IMU, pressure depth sensor, and single beam echosounder, the research highlights the superiority of the pressure sensor and tide information over GNSS PPK-derived height. The study underscores the value of echosounder point cloud data for survey improvement and DSM height correction, emphasizing the importance of reliable camera calibration in achieving accurate results.

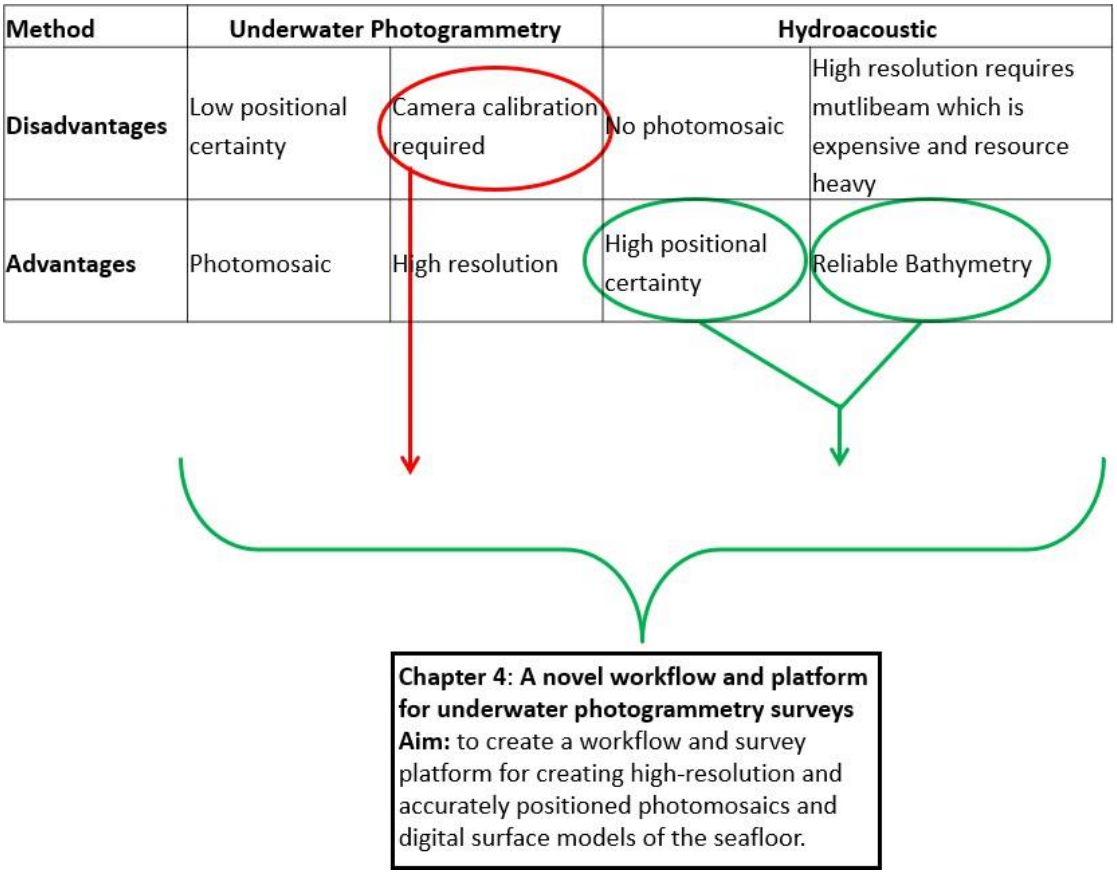

Mufti, A., Helmholz, P., Belton, D., Allahvirdi-Zadeh, A., & Parnum, I. (2024). A novel platform and workflow for underwater photogrammetry surveys. *International Annals of the Photogrammetry, Remote Sensing & Spatial Information Sciences*, Midterm-symposium commission IV, submitted, decision pending.

A novel platform and workflow for underwater photogrammetry surveys

Alaa Mufti [1, 2, 3], Petra Helmholz [1], David Belton [1,], Amir Allahvirdi-Zadeh [1] and Iain Parnum [1, 2]

[1] School of Earth and Planetary Sciences, Curtin University, Bentley, Western Australia
GPO Box U1987, Perth WA 6845, Australia, alaa.mufti@postgrad.curtin.edu.au, (P.Helmholz, D.Belton, Amir.Allahvirdizadeh, I.Parnum)@curtin.edu.au
[2] Centre for Marine Science and Technology, Curtin University, Bentley, Western Australia
[3] King Abdulaziz University, Rabigh 25732, Saudi Arabia

KEYWORDS: Underwater Photogrammetry, Calibration, GNSS PPK, single beam echosounder.

ABSTRACT
Underwater photogrammetry has gained popularity for creating three-dimensional (3D) maps and ortho-images of marine environments as compared to traditional echosounder surveys, they can be more cost-effective at creating high-resolution 3D models, and orthoimages are usually more informative than acoustic backscatter maps. This paper builds on previous work by the authors that developed an underwater image-capturing platform with several additional sensors, including GNSS, IMU, pressure depth sensor and single beam echosounder. This study aims to analyse the impact of calibration and sensor data integration into the photogrammetric processing workflow. The tests were performed using two underwater sites. The low-cost device's pressure sensor and tide station data outperform GNSS PPK-derived heights. Furthermore, it was observed that incorporating IMU motion sensor data did not improve the processing results. Additionally, utilising the echosounder point cloud proves valuable for enhancing the overall quality of the survey. Despite its lower density, it serves a dual purpose by validating the photogrammetry dataset and, more importantly, can be employed for correcting DSM height. This study further underlined the importance of reliable camera calibration for accurate 3D reconstruction.

Introduction

Accurate maps of bathymetry and seafloor habitat, allow for the prediction and mitigation of various environmental impacts (Pickrill and Todd, 2003). Thus, the evolution of underwater mapping and monitoring technology enhances our potential understanding of the sea and coastal areas, benefiting management efforts. Mapping the marine environment has traditionally been carried out via aerial and satellite remote sensing or vessel-based echosounder surveys (Parnum et al., 2009; Brown et al., 2011). More recently, underwater photogrammetry has gained popularity for creating three-dimensional (3D) maps and ortho-images of marine environments (Nocerino et al., 2020). It can be carried out by scuba divers and remotely operated or autonomous underwater vehicles (Mahrad et al., 2020, Rofallski et al., 2020). However, achieving high accuracy in the geolocation and scale of underwater models generated from photogrammetry can be more challenging than terrestrial environments. This is because calibration and positioning methods are more difficult for underwater surveys, which can mean the interior and/or exterior orientation parameters are not adequately calculated. Additional sensor data must be integrated with the images, offering a georeferenced location and a point cloud (Rofallski et al., 2020).

This paper builds on previous work by the authors that developed an underwater image-capturing platform that uses open-source devices to log the position and motion of the rigid camera frame using several sensors installed on the platform (Mufti et al., 2023a). The platform is designed to conduct underwater photogrammetry surveys. The motivation of this study is to use the advantages of traditional single-beam echosounder surveys and contemporary underwater photogrammetry methods, effectively addressing the inherent limitations of each approach. Specifically, the aim is to leverage the precise GNSS positioning and reliable bathymetric data acquired through single-beam surveys. This information is used as a robust reference framework for enhancing the accuracy of the photogrammetry workflow. The synergy between these methodologies is designed to overcome the constraints associated with standalone single-beam surveys and photogrammetry techniques. By combining these traditional and contemporary survey methods, the study offers a novel approach that not only mitigates their individual limitations but also unlocks new possibilities in underwater mapping and visualization.

This study aims to analyse the impact of calibration and sensor data integration into the photogrammetric processing workflow. In other words, additional information captured by the imaging platform is used to constrain the image processing pipeline. The study area of this paper is an area with artificial reef structures close to the shoreline. The resulting 3D models of these artificial reefs are compared to bathymetric multibeam survey data of the area and an aerial ortho-image of the structures to evaluate the performance of the calibration frame and the positioning methods.

The paper is structured as follows: In section 2, we will briefly review the platform introduced in Mufti et al. (2023a) and the study area. Next, in section 3, we will introduce the method for processing the sensor and image data captured from an underwater photogrammetry survey of the artificial reef. In section 4, we validate outputs. The paper concludes with a conclusion and outlook in section 5.

Platform and study area

Mufti et al. (2023a) introduced a platform (Figure 1) to collect ancillary data for underwater photogrammetry surveys. The platform carries the sensors as presented in Table 1. It uses a Raspberry Pi to collect time-synchronised data, including (X, Y, Z) position, depth, altitude and motion.

In this study, three GoPro 5 cameras were mounted to the platform's rigid frame, positioned underwater just below the surface (Figure 1). These GoPro 5 cameras were used as they have been shown to perform well when used for underwater photogrammetry (Helmholz et al., 2016).

The platform with mounted cameras was used to conduct an underwater photogrammetry survey of sublittoral artificial reefs in Coogee Beach, near Omeo Wreck, West Australia (WA) (-32.105189o E, 115.761165o S) on the 26th of August 2023. Two study areas (1 and 2) were chosen for analysis and are shown as white polygons in Figure 2. Figure 2 also shows part of the platform track. The ortho-image and multibeam bathymetry captured in 2021 by the WA Government are shown in Figure 2 (at 10 cm grid size). The multibeam bathymetry was the closest in time to our survey in 2023, and the ortho-image had the best visibility in recent aerial surveys.

	Type	Product	Measuring of
1	GNSS	SparkFun GPS-RTK Board – NEO-M8P-2 Receiver	Location and altitude
2	Pressure sensor	BlueRobotics Bar30 High-Resolution 300m Depth/Pressure Sensor	Depth
3	IMU	Raspberry Pi Sense HAT V2	Motion
4	Single-beam echosounder	BlueRobotics Ping Sonar Altimeter and Echosounder	Sparse point cloud
5	Cameras	GoPro Hero 5 (set to 4000 x 3000 pixels, f/2.8, 1/330 sec exposure and ISO-100)	Images

Table 1. Overview of sensors on data capture platform.

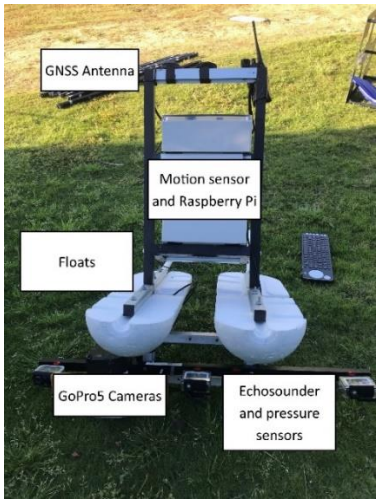

Figure 1. Platform used to carry out underwater photogrammetry and echosounder surveys.

Methods

In this section, we will introduce the processing of the sensor data, followed by a description of the image processing pipeline. The aim is to apply a standard photogrammetric processing pipeline but to constrain the adjustment by utilising the sensors that are part of the capturing platform.

Sensor data processing

GNSS processing

The platform has a built-in Global Navigation Satellite System (GNSS) receiver that can be used to obtain the platform's location when images are captured. The location information can be used to constrain the image processing pipeline. Mufti et al. (2023a) concluded that GNSS post-processing kinematic (PPK) provides the best position information available for the image processing pipeline. Hence, this method is applied here.

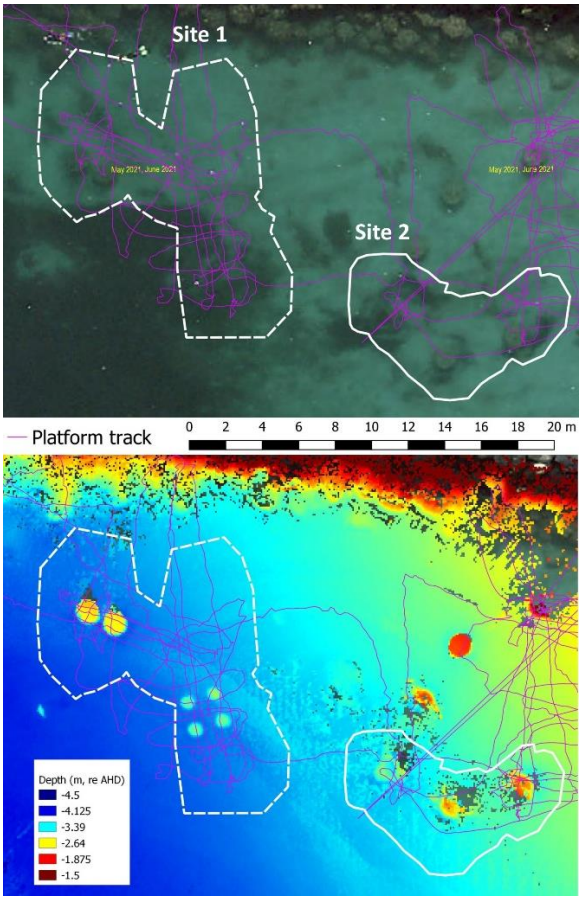

Figure 2. Platform tracks of the underwater photogrammetry survey (in magenta) over an aerial photo (top) and multibeam bathymetry (bottom). The two white polygons show the location of study areas 1 (dashed line) and 2 (solid).

As there were no existing survey marks near the survey area, a base station was established < 100 m from the survey area, using a Trimble R12 receiver logging for three and half hours in static mode. The base station was used to log data to enable PPK to be carried out. The data collected at the base station was processed using a long-baseline approach using the Australian Online GPS Processing Service (AUSPOS) developed by GeoScience Australia (https://gnss.ga.gov.au/auspos). The 95% positioning uncertainty of the base stations following AUSPOS processing was 0.014 m (X-Y) and 0.167 m (Z). Analysis of the X-Y positioning data showed a difference of 10-30 cm in absolute position (accuracy) in places, which was consistent with Mufti et al. (2023a). The raw GNSS code and phase observations from the platform were processed with the adjusted base station data, using RTKLIB to carry out PPK (Takasu, 2013). Data were exported in Map Grid of Australia (MGA50) and heights re Australian Height Datum (AHD).

Pressure sensor measurements

As an alternative method of estimating the elevation of the platform, it is possible to use the pressure sensor installed on the platform. The pressure data was converted to a depth using the standard UNESCO endorsed formula, and then corrected for tide using measurements from the WA Government tide station at Fremantle Fishing Boat Harbour 6 km away. As the tide measurements were relative to chart datum (CD), an offset of 0.756 m was applied to transfer these values to AHD.

Motion data
Other measurements that can constrain the photogrammetric workflow are the motion information captured by the inertial measurement unit (IMU) installed onto the imaging capturing platform. A series of simple calibration exercises were carried out to calculate values of roll, pitch, and yaw relative to the frame and in the convention used in the photogrammetry workflow. The yaw was also corrected for magnetic declination, as the heading sensor was a magnetic compass.

Single-beam echosounder depths
The single-beam echosounder data collected by the platform during the survey was time-tagged with the PPK position data and corrected for sound velocity and physical offsets. The seafloor depth was calculated in two ways: 1) by reducing the soundings with the pressure sensor data and tide observations as per Mufti et al. (2023a), and 2) by using the PPK heights. Both were exported as a point cloud referenced re AHD. The derived sparse point cloud was investigated to add constraints to the image processing pipeline and as a correction post-photogrammetry workflow.

Image processing

Photogrammetric workflow
Photogrammetric 3D reconstructions were carried out using Bentley's Context Capture (CC) software (v10.19.0.122). The processing pipeline followed a classical photogrammetric processing workflow, including the initial alignment of all images based on automatically extracted feature points, the inclusion of control as per the processed dataset, a least squares bundle block adjustment, followed by the creation of dense point clouds, meshes and ortho-images (ortho-images). The least squares adjustment was constrained by the different inputs of the other sensors. An overview of the different constraints is provided in Table 2. For instance, the least squares adjustment can be performed using an X, Y, and Z constraint on the platform's location based on the GNSS PPK results. However, the Z component can also be used from the pressure sensor corrected for tide. All Z values are in the AHD to make the results comparable.

	Sensor data used	Constraint applied
1	GNSS PPK	X, Y, Z
2	Pressure sensor (+ tide)	Alternative solution Z
3	IMU	Pitch, Roll, Yaw
4	Single-beam echosounder	Dense Point Cloud

Table 2. Constraints to the bundle adjustment.

A Digital Terrain Model (DTM) was also created from the Digital Surface Model (DSM), by manually removing the artificial reefs from the data in CloudCompare (2.12 beta). Finally, ortho-images were created using CC. All relevant parameters are presented in Table 3.

	Process	Parameters
1	Dense Image matching	Resolution: 0.0011 m Projection mode: Highest point
2	Ortho-image	Ground Sample Distance: 0.01 m

Table 3. Utilised parameters for the image processing.

Camera calibration
In addition, three different methods of camera calibration are applied to the images. Next to the self-calibration based on the images captured (selfCal) two calibration frames are utilised. The two frames were introduced in Mufti et al. (2023b) - rigid cube (Figure 3, left), and a collapsible pyramid (Figure 3, right). Both were submerged near the test area, and several images were taken while collecting the main data. The camera is calibrated based on those images, and the camera calibration parameters are applied when the images of the test sites are processed. An overview of the calibration methods is provided in Table 4.

	Calibration	Explanation
1	selfCal	Self-calibration based on the images captured of the test sites
2	calC	Calibration using cube frame
3	calP	Calibration using collapsible pyramid

Table 4. Calibration methods allied during image processing.

The camera calibration parameters that are solved are focal length (*c*), principal point offset (*XP, YP*), radial lens distortion parameters (*k1-k3*), and decentring distortion parameters (*p1, p2*). The camera calibration parameters are calculated during the pre-calibration and then applied during further processing.

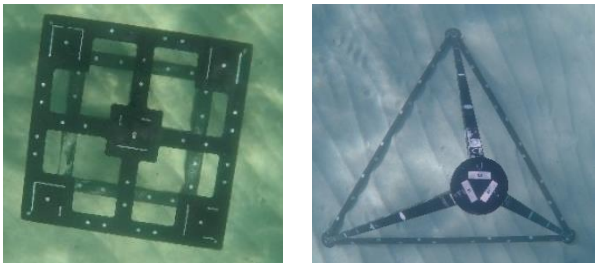

Figure 3. Calibration frame for the pre-calibration of the camera. Cube (left) and collapsible pyramid (right).

Evaluation

For the evaluation, a multibeam bathymetry dataset was available. The multibeam bathymetry was captured in 2021 by the WA Government. This is a challenge as the site has changed between 2021 and 2023. For instance, additional structures were submerged, and the ocean seafloor (sand) has changed. However, due to the lack of any other reference data, we had to utilise this slightly outdated dataset.

When point clouds are compared, a point-to-surface comparison between the different clouds is performed, whereas the surface is defined by the 8 nearest neighbour points. No alignments of the point clouds were performed for geo-referenced datasets. The resulting distances are shown in histograms through which a Weibull distribution is fitted. The metrics used to quantify the differences between the point clouds are provided in Table 5. For the comparisons, CloudCompare was utilised.

Camera calibration

Comparison of results using the two different fames
Firstly, we want to establish if there are significant differences when applying the calC and calP methods. The results of calibrating the three GoPro 5 cameras using these two methods are summarised in Table 6. The GNSS location and pressure and tide information for depth were also utilised for both datasets. Using the calP for the calibration, produced results with a reprojection error (RMS) of 2.05 pixels and the RMS of distances to rays of 3.6 mm. The calC performed better, with a reprojection error (RMS) of 1.4 pixels, and a RMS of distances to rays of 2.9 mm.

The calP structure did not perform as well as it did in Mufti et al. (2023b). A possible reason is the geometry in which the images were captured. Figure 4 shows clearly that the camera stations during the capture of calP are closer to each other, consequently leading to not justifying calibration results. This highlights the significance of

careful selection of the configuration camera stations during the data capture.

Parameter	Explanation
Weibull shape parameter *a*	A large *a* means the distribution is moved away from zero, so significant distances are present between the compared point clouds.
Weibull scale parameter *b*	0 < *b* < 1, the larger the number, the distribution is more stretched out.
95% confidence interval [m]	It determined the distance in which 95% of the calculated distances fall.
Mean, Mode [m]	The Mean and Mode of the point cloud distances.
Shift (X, Y, and Z) [m], Scale	If the locations of two different point clouds are compared, their shift vector and their different scales are compared.
STD, RMS [m]	Standard deviation (STD) between the mean and samples as well as Root Mean Squared (RMS) of the alignment.

Table 5. Parameters used in the comparison of point clouds.

Camera	RE	D2R	#images	F	XP	YP
calC						
Left	1.4	2.9	128/175	20.94	1998	1493
Mid	1.4	2.9	97/144	20.8	1992	1493
Right	1.4	2.9	146/232	20.78	2028	1481
calP						
Left	2.05	3.6	39/42	21.16	1993	1491
Mid	2.05	3.6	16/26	21.61	2095	1582
Right	2.05	3.6	81/83	21.19	2037	1490

Table 6. Parameters from the pre-calibration of three cameras (Left, Mid and Right) using the Cube and Pyramid frames. The focal length (F) is provided as Equivalent 35 mm. XP and YP are the principal point offsets in X and Y provided in pixels. D2R = Distance to rays (mm). RE = Reproj. (RMS) pixels.

The impact of the not optimal camera station layout during the data capture for calP is likely to be the source for the quite different camera calibration parameters (Table 6). For instance, the focal length of calC is constantly shorter than using calP for all three cameras used (Table 6).

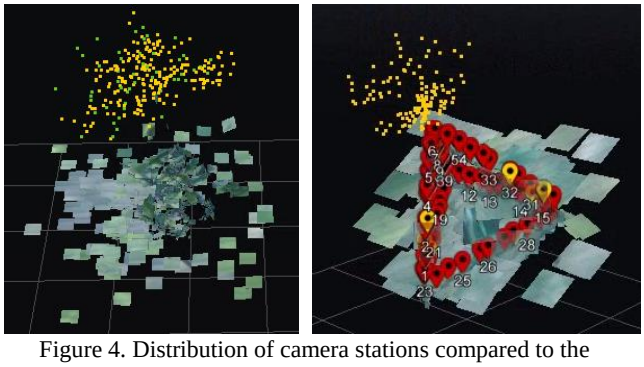

Figure 4. Distribution of camera stations compared to the calibration frame (Left: calC, Right: calP).

Self-Calibration (selfCal) with and without additional sensor information

In contrast to the pre-calibration using the calC or calP method, it is also possible to perform a self-calibration based on the images captured from the test sites. Self-calibration is known to create a bowing or doming effect if the data capture is not performed in a geometry suitable for self-calibration, e.g. using orbital "flights" with high overlap. While it is possible to perform well-considered and easy-to-execute flight planning for in-air applications (e.g. for drones), this is not always the case underwater.

The outcomes of the self-calibration performed for test site 2 are detailed in Table 7. For this test, only the results of site 2 are presented, and are comparable to the results of test site 1. Using the test site 2 dataset, two different tests are performed. Firstly, a self-calibration is performed without additional constraints such as Sensor Data (SD) (selfCal-NoSD). This means no GNSS and depth sensor data is used. The second self-calibration uses the GNSS location data and additional pressure and tide data for depth measurements (selfCal-WithSD). The utilisation of additional sensor information is hoped to enhance the calibration's robustness and reliability, contributing to more accurate and meaningful results in the subsequent analysis. However, Table 7 does not show any indicators for a more reliable calibration when adding the sensor data (GNSS X, Y), pressure sensor and tide (Z). The reprojection errors are similar, and the focal length as well as XP and YP, are comparable. The results are even comparable with the calibration results achieved by calC and calP in Table 6. The only difference is a slightly different focal length.

Camera	RE	D2R	#images	F	XP	YP
self-Cal with no additional Sensor data (NoSD)						
Left	1.3	0.06	239/ 244	21.27	2019	1486
Mid	1.3	0.06	246/ 252	21.3	2006	1488
Right	1.3	0.06	248/ 253	21.33	2022	1487
self-Cal with additional Sensor data (WithSD)						
Left	1.4	0.02	177/ 178	21.24	2007	1492
Mid	1.4	0.02	179/ 188	21.3	1996	1497
Right	1.4	0.02	170/ 170	21.33	2014	1497

Table 7. SelfCal parameters with no and with additional sensor data for the three cameras (Left, Mid and Right) calculated based on test site 2. The focal length (F) is provided as Equivalent 35 mm. XP and YP are the principal point offsets in pixels. D2R = Distance to rays (mm). RE = Reproj. (RMS) pixels.

Pre-calibration vs self-calibration

Next, we compare the estimated parameters for pre- and self-calibration. A special focus is given to the radial lens distortion, as those are correlated with the appearance of the bowing/doming effect. The radial lens distortion profiles for calP, calC, selfCalWithSD and selfCalNoSD of the right camera are shown for site 1 Figure 5. The largest correction values are always present for the CalP method (blue profile). The CalC method (grey profile) is "in-between" the CalP and the selfCal methods. The selfCal methods with (selfCalWithSD, yellow profile) and without (selfCalNoSD, orange profile) sensor data have very similar profiles. The left camera produces a very similar radial lens distortion plot (not shown). However, the centre camera shows a stronger alignment of the selfCal methods with (selfCalWithSD) and without (selfCalNoSD) sensor data for both site profiles to CalC (not shown). This could be explained by the different viewing angles of the centre camera compared to the right and left cameras.

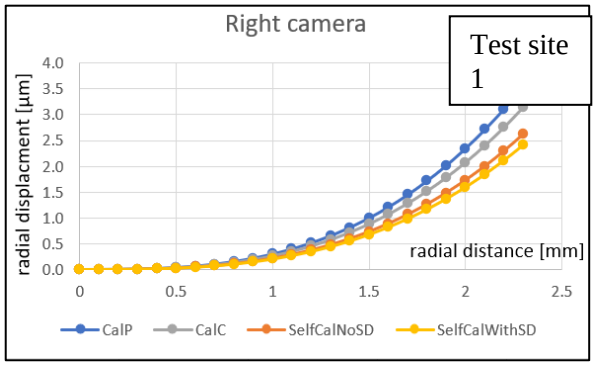

Figure 5. Radial lens distortion profiles of the right camera using the different calibration methods, test site 1.

Sensor data impact on DTM and DSM products

Further investigations regarding the impact of the calibration parameters on the derived DTM/DSM are presented in the next section.

Impact of different camera height information

Due to the sensors installed on the platform, the depth of the cameras (i.e. their elevation re AHD) information can be derived using two methods. One was using the elevation data from the GNSS PPK, and the other using the pressure and tide station data. The impact of the different depth inputs was quantified using the DTMs produced using these methods, compared with the reference multibeam data. Due to the low quality of the multibeam data from the shallower site 2, only site 1 was compared. As site 2 changes between when the multibeam data was captured to our data collection (new artificial reefs were added), we are comparing the DTM and not the DSM.

The site 1 DTM produced using the constraint of the pressure & tide data was closer to the reference surface, than the DTM produced using the PPK elevation, both visually (Figure 6) and in performance metrics (Table 8). For instance, the mean difference between the multibeam surface and the DTM produced using the pressure & tide data was 6 cm, compared to 27 cm for the DTM produced using the PPK height (Table 8).

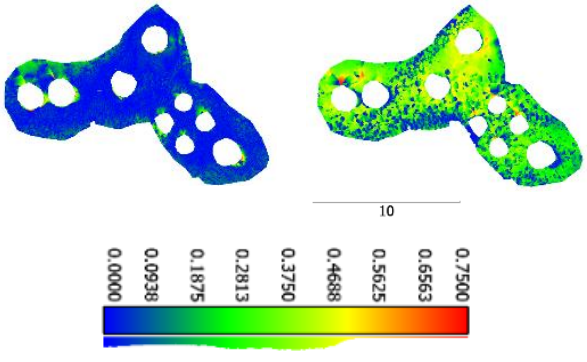

Figure 6. Comparing DTMs for site 1 produced using pressure sensor and tide data (dataset 4, left), and PPK height (dataset 2, right) vs multibeam. In meters.

Dataset	95% [m]	a	b	Mode [m]	Mean [m]	STD [m]
PPK height	0.48	1.71	0.29	0.37	0.27	0.14
Pressure & tide	0.21	0.95	0.06	0.0	0.06	0.08

Table 8. Comparison results of the DTM derived from PPK height and pressure and tide vs multibeam for test site 1.

Impact of the combination of calibration method and different depth information on the DSM

Previously, we established that the calibration method and the depth information can impact the results of the reconstruction significantly. The best results have been achieved using calC and GNSS positioning outputs (X,Y) with pressure and tide for elevation (Z). We have also established that adding sensor information has little impact on the selfCal result of the camera calibration parameters. While the camera calibration parameters (besides the radial lens distortion profiles) are very similar, we now try to establish if adding location and depth data into the processing has an impact on the resulting DSM. For the analysis, we utilise the test site 2 results. The reference used was the dataset processed with the best-performing methods so far (calC, GNSS positioning outputs (X,Y), pressure and tide for elevation (Z)).

We are going to compare the reference dataset to the following:

1. Dataset 1: self-cal with pressure sensor and tide
2. Dataset 2: self-cal with PPK Height
3. Dataset 3: Pre-Calibrated (Cube) with PPK height

The results of the comparison are shown in Table 9. In comparing these scenarios against the reference dataset, dataset 3 demonstrates superior performance, with a significantly smaller 95% confidence interval (0.09 m vs 0.57 m and 0.16 m). The RMS error is also significantly lower (0.083 m vs 0.187 m and 0.192m). However, it must also be highlighted that introducing additional location and depth information into the self-calibration improves the results.

Remarkable is the shift in z-direction (Table 9), which for the self-calibration datasets (-0.076 m and -0.481 m) is very different from the pre-calibrated dataset (0.228 m). Firstly, the sign is the opposite, and secondly, the magnitude is much larger. It is known that any calibration error impacts the depth estimation, which can be seen to be clearly the case here.

The results suggest that DSMs produced using pre-calibration (and camera height), are more accurate and precise data than self-calibration (with camera height data), making it the preferred method. The effectiveness of pre-calibration is evident in the smaller deviations from the reference, highlighting its potential for enhancing the accuracy and reliability of positioning data in underwater photogrammetry applications.

Comparing the DSM point clouds of dataset 1 to dataset 3 to the reference (Figure 7) clearly shows the strong bowing of the selfCal datasets (1 and 2). For this comparison, the shift presented in Table 9 has been eliminated, but the scale has not been adopted. The bowing effect is mostly in the north/south direction. For dataset 2, the bowing is also in the east/west direction. The area indicated by the black arrow in Figure 7 exceeded the defined limit of 0.6m and is, for this reason, not presented. In contrast, dataset 3 shows only a small bowing effect, again in the north-south direction, but in the opposite direction of datasets 1 and 2. The resulting bowing/doming effect due to incorrect radial lens distortion parameters, is in line with the results of other researchers (Carbonneau & Dietrich, 2017; Habib et al., 2005).

	1. Self- cal., pressure & tide	2. Self- cal., PPK Height	3. CalC., PPK height
95% [m]	0.57	0.16	0.09
a	1.0381	0.986	0.9728
b	0.1891	0.175	0.0261
Mode [m]	0.002	0.002	0.005
Mean [m]	0.186	0.176	0.026
STD [m]	0.179	0.189	0.029
Shift x [m]	-0.067	-0.086	0.065
Shift y [m]	0.099	0.048	0.050
Shift z [m]	-0.076	-0.481	0.228
Scale [m]	1.036	1.030	1.002
RMS [m]	0.187	0.192	0.083

Table 9. Comparison results of the DSM derived from different combinations of calibration and depth information.

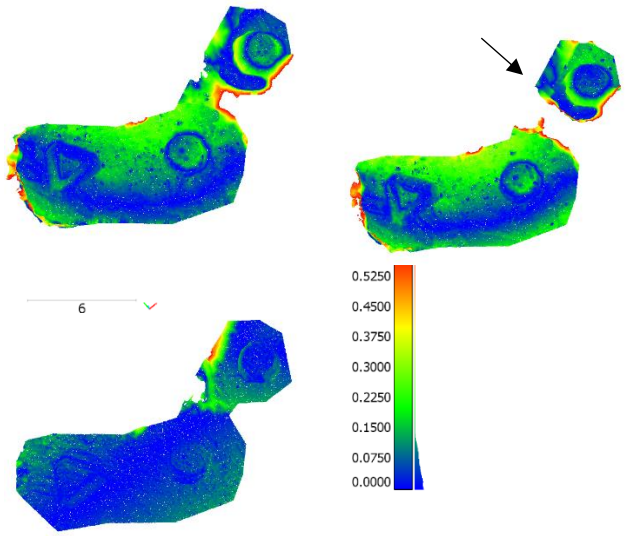

Figure 7. DSM of the reference dataset with dataset 1 (top right), dataset 2 (top left) and dataset 3 (bottom).

Impact of Motion Data

To assess the impact of motion data on the calibration process, two scenarios were compared: self-calibrated with pressure sensor and tide with motion and self-calibrated PPK height with motion. The reference dataset is the same as in the previous test (in 4.2.2), so cube pre-calibration and using pressure and tide for elevation. The results are presented in Table 10. Again, the results using pre-calibration outperform the dataset with self-calibration. The 95% confidence interval is less than half (0.164m vs 0.096m). However, the difference is not as much as the previous test, e.g. only 1.2 cm between their mean differences with the reference surface. Interestingly, the RMS values for the self-calibration improved when adding motion information (Table 9: 0.187m vs 0.143m in this test), but the RMS increases for the pre-calibrated dataset: 0.083m vs 0.193m in this test (Table 9 and Table 10).

A possible reason for the motion information to decrease the accuracy is the environment. The sensor is surrounded by metal and other sensors that could potentially interfere with data collection and the presence of small waves and pumps in the models was attributed to the waves on the seafloor. A more rigorous calibration of the IMU, or the use of an array of GNSS antennae, is expected to improve the results but is outside of the scope of this paper.

	Self- cal., pressure & tide with motion	Pre-Cal PPK height with motion
95% [m]	0.164	0.096
a	0.8331	1.1350
b	0.0427	0.0351
Mode [m]	0.001	0.008
Mean [m]	0.047	0.035
STD [m]	0.063	0.031
Shift x [m]	0.053	-0.019
Shift y [m]	0.035	0.077
Shift z [m]	-0.024	0.203
Scale [m]	1.029	0.989
RMS [m]	0.143	0.193

Table 10. Comparison results of the DSM derived from different combinations of depth information together with added motion information.

Impact of single-beam depth data

The single-beam depth data can be used to create a sparse point cloud, which can also be used to constrain the least squares adjustment, and outside of the photogrammetry workflow to validate and/or adjust the 3D models.

Validation of single-beam depth data using multibeam data

As the first step, we analyse the quality of the Single-beam depth data by comparing the data to the multibeam dataset, using both vertical reduction methods. The data agreed well with the historic multibeam bathymetry (Figure 8). The correlation was slightly higher (R = 0.88) and RMS slightly lower (0.33 m) for the soundings reduced using tide, compared to using the PPK Height (R = 0.86, RMS = 0.34 m).

Comparison of elevation vs echo-sounder altitude for camera heights

The use of the single beam data was investigated as a way to position the camera's height as an altitude (as opposed to the previously used elevation) in the photogrammetry workflow. The DSM generated from this approach was compared with the, so far, best-performing dataset processed using CalC, GNSS location outputs (X,Y), and pressure & tide depth data (Z, i.e. elevation) without motion information. The provided numerical breakdown (Table 11), shows that the camera height is better referenced as an elevation than altitude in the workflow, with a 95% confidence interval ranging from 1.7 to 2.5 m. The mean value of 2.56 m and the standard deviation of 0.40 m (Table 11), illustrate the exterior orientation parameters determined by the photogrammetry workflow are better when it derives the altitude, rather than images being tagged with it.

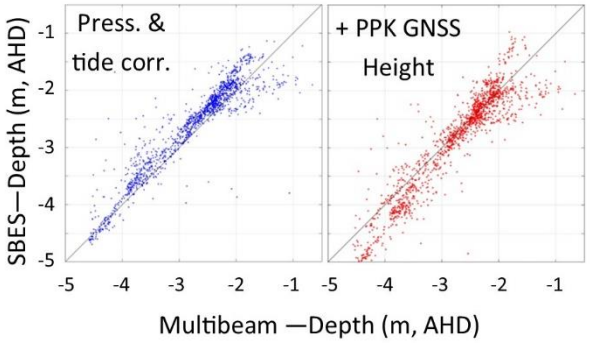

Figure 8. Single beam echosounder (SBES) depth values from this survey compared to historic multibeam depths collected in 2021: Left: soundings reduced using the pressure and tide, Right: soundings referenced using the PPK height.

	95% [m]	a	b	Mode [m]	Mean [m]	STD [m]
SBES	2.73	8.52	2.5	2.6	2.4	0.40

Table 11. Comparison of single-beam echo-sounder (SBES) depth data vs photogrammetry

Integrating the single-beam beam data into the photogrammetry workflow

The integration of the single beam depth data into the photogrammetry workflow was investigated. However, CC software omitted the single beam point cloud in the workflow, citing its lower density. This led to an additional layer beneath the photogrammetry point cloud, as shown in Figure 9. The exclusion of the single beam data indicates the software's preference for higher-density datasets, which aim to bolster the fidelity and detail of the resulting reconstructions by strategically leveraging photogrammetric and echosounder datasets.

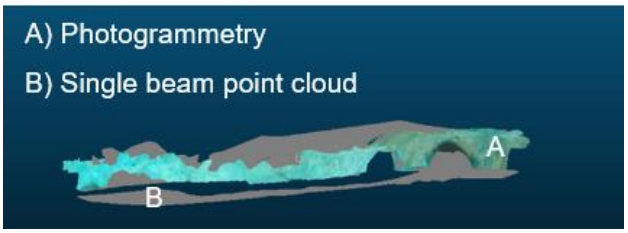

Figure 9. Fusion of echosounder data with photogrammetry.

Validation of using single beam data to correct DSMs that used GNSS heights

We evaluated whether the single-beam echosounder (SBES) depths can improve the accuracy of the DSM, post-photogrammetry workflow. In previous tests, the PPK height information achieved constantly worse results compared to the datasets processed with pressure and tide. In this test, the DSM derived using PPK heights is corrected using the SBES depth data. Hence, the following datasets are processed and then compared to the multibeam reference dataset:

- dataset 1: CalC, GNSS (X, Y, Z), no motion data
- dataset 2: CalC, GNSS (X, Y), pressure & tide (Z), no motion data
- dataset 3: Same as Dataset 1, then the resulting DSM has its Z value corrected using linear regression against the SBES.
-

The results are presented in Table 12, show that Dataset 1, representing PPK height, had a higher mean difference with the reference surface (24.8 cm) compared to dataset 2, which represents pressure and tide (14.7 cm). However, a corrected PPK height using linear regression with the SBES depth data (dataset 3), had a mean difference of 17.4 m. This represents a notable improvement over dataset 1, reducing the mean error by 30%. The effectiveness of the SBES correction applied post the photogrammetry workflow, can be further seen by visually comparing the multibeam depth (Figure 10a) with the DSMs of datasets 1 (Figure 10b) and 3 (Figure 10c), and SBES depths (Figure 10d).

	dataset 1	**dataset 2**	**dataset 3**
95% CI [m]	0.491	0.590	0.597
a	1.465	0.797	0.948
b	0.271	0.128	0.170
Mode [m]	0.015	0.016	0.002
Mean [m]	0.248	0.147	0.174
STD [m]	0.155	0.195	0.192

Table 12. Comparison results of the DSM derived from different combinations with multibeam reference dataset.

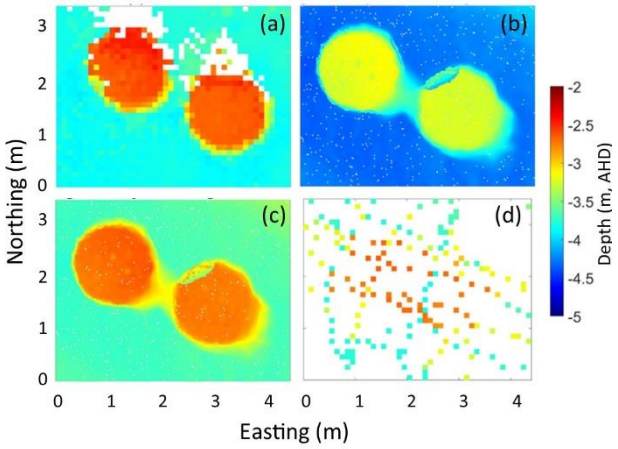

Figure 10. (a) multibeam data. B) photogrammetry with incorrect depths. C) photogrammetry – with SBES correction. D) SBES depth.

Photo mosaics

Photo mosaics generated using the combination of cube calibration and pressure sensor and tide for camera height (as well as PPK for camera X-Y positioning), for site 1 and site 2 are shown in Figure 11. Compared to the multibeam and aerial ortho-image captured in 2021 (Figure 2), two of the round "Bomboras" in site 1 are not present, as it appears they have not been deployed, yet. The difference between the location of the reef structures in multibeam and aerial captured ortho-image in (Figure 2), and the photo mosaics in Figure 11 is < 30cm. This was without any GCPs. Additionally, in the aerial-captured ortho-image, it is hard to make out the group of four "Apollo" (Figure 2), compared to the ortho-image produced in this study (Figure 11). This is due to a combination of the water surface impeding the aerial image capture, and the higher resolution of this study due to the cameras being closer to the survey area. This highlights the advantage of capturing images underwater compared to an above-water aerial platform. In addition, Site 2 is quite shallow (< 3 m), as a result, the multibeam data is sparser and noisier (than site 1), meaning the structures are less defined than the photogrammetry DSMs. This highlights an advantage of using photogrammetry over multibeam echosounders in very shallow water.

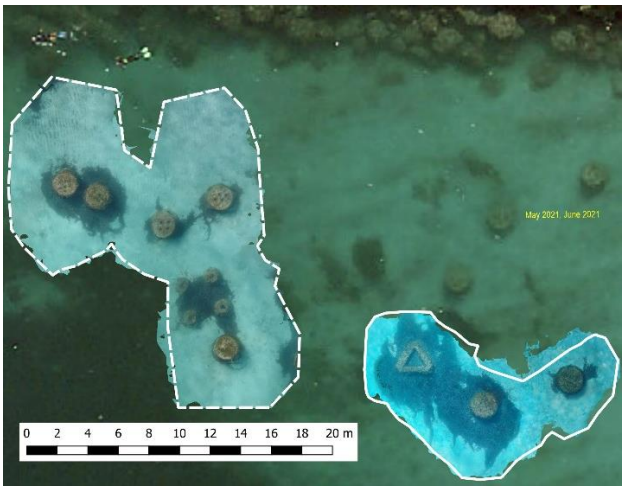

Figure 11. Ortho-images generated for site 1 (left) and site 2 (right) over an aerial photo.

Conclusion and Further work

The challenges of underwater photogrammetry surveys, particularly in achieving accurate calibration and precise positioning, can often lead to inaccuracies in determining interior and exterior orientation parameters. This study addresses these challenges by building upon prior research by the authors. The survey platform (Mufti et al, 2023a) and camera calibration frame (Mufti et al, 2023b) previously developed, were employed in an underwater photogrammetry survey on an area featuring artificial reef structures. The 3D models generated from this survey were validated using bathymetric multibeam survey data. This comparison aimed to assess the effectiveness of using a calibration frame and the positioning methods, specifically evaluating their impact on the accuracy of geolocation and scaling in the context of underwater photogrammetry.

Carrying out a pre-calibration using a dedicated 3D structure, produced more accurate 3D models than the self-calibration method. This is consistent with other studies (Shortis, 2019). Of the two calibration frames tested, the rigid cube outperformed the collapsable pyramid. Reasons for this might be the geometry in which the images were captured, or the collapsable frame might not be consistently rigid.

The impact of the sensor data derived from the platform on the photogrammetric processing was analysed. Among these, the pressure sensor measurements combined with and tide station, emerged as more effective in accurately tagging the camera height than GNSS PPK height.

It was observed that incorporating the motion sensor data did not improve the processing results. However, the calibration of the sensor and the use of high-grade IMUs, especially using a secondary GNSS antenna, should be considered in future studies.

Although the single beam depth point cloud could not be incorporated in the photogrammetry workflow, due to its relatively low density, proved valuable for enhancing the overall quality of the survey. Despite its lower density, it can serve the dual purpose of validating DSM heights, and where necessary, correcting the heights of DSMs.

We concluded an optimal workflow for this study was to: carry out a dedicated, in-situ pre-calibration using a rigid 3D structure; tag images with GNSS PPK X-Y positions; use pressure sensor and tide station measurements for the camera height; and collect echosounder data to enable validation and as a fail-safe for correcting any erroneous heights. Using this approach produced a DTM that had an RMS of 6 cm compared to multibeam, and a geolocation error of < 30cm. This was done without the use of GCPs, which are challenging to create in an underwater setting. This study, thus, has presented the notable benefits of pre-calibration of cameras using a 3D structure, and the integration of single-beam bathymetry into the photogrammetry workflow.

Acknowledgements

The authors would like to thank King Abdulaziz University for funding Alaa Mufti's PhD study, and Mr Malcolm Perry and Mr Ming Lim from Curtin University for technical support. We also thank Curtin's 3D Hub for the opportunity for the data processing.

References

Brown, C. J., Smith, S. J., Lawton, P., & Anderson, J. T. 2011. Benthic habitat mapping: A review of progress towards improved understanding of the spatial ecology of the seafloor using acoustic techniques. Estuarine, Coastal and Shelf Science, 92(3), 502-520.

Carbonneau, P. E., & Dietrich, J. T. 2017. Cost-effective non-metric photogrammetry from consumer-grade sUAS: implications for direct georeferencing of structure from motion photogrammetry. Earth Surface Processes and Landforms, 42(3), 473-486.

Habib, A., Ghanma, M., Morgan, M., & Al-Ruzouq, R. 2005. Photogrammetric and LiDAR data registration using linear features. Photogrammetric Engineering & Remote Sensing, 71(6), 699-707.

Helmholz, P., Long, J., Munsie, T., & Belton, D. 2016. Accuracy assessment of go pro hero 3 (Black) camera in underwater environment. The International Archives of the Photogrammetry, Remote Sensing and Spatial Information Sciences, 41, 477-483.

Mahrad, B. E., Newton, A., Icely, J. D., Kacimi, I., Abalansa, S., & Snoussi, M. 2020. Contribution of remote sensing technologies to a holistic coastal and marine environmental management framework: a review. Remote Sensing, 12(14), 2313.

Mufti, A., Parnum, I., Belton, D., & Helmholz, P. 2023a. An open-source, data-logging device for marine-based surveys. International Archives of the Photogrammetry, Remote Sensing & Spatial Information Sciences, II WG II/7.

Mufti, A., Parnum, I., Belton, D., & Helmholz, P. 2023b. introduction and validation of a novel calibration frame. International Archives of the Photogrammetry, Remote Sensing & Spatial Information Sciences, II WG II/7.

Parnum, I., Siwabessy, J., Gavrilov, A., & Parsons, M. 2009. A comparison of single beam and multibeam sonar systems in seafloor habitat mapping. In: Proc. 3rd Int. Conf. and Exhibition of Underwater Acoustic Measurements: Technologies & Results, Nafplion, Greece (pp. 155-162).

Pickrill, R. A., & Todd, B. J. 2003. The multiple roles of acoustic mapping in integrated ocean management, Canadian Atlantic continental margin. Ocean & Coastal Management, 46(6-7), 601-614.

Rofallski, R., Tholen, C., Helmholz, P., Parnum, I., & Luhmann, T. 2020. Measuring artificial reefs using a multi-camera system for unmanned underwater vehicles. International Archives of the Photogrammetry, Remote Sensing and Spatial Information Sciences-ISPRS Archives, 43(B2), 999-1008.

Shortis, M,. 2019. Camera calibration techniques for accurate measurement underwater. 3D recording and interpretation for maritime archaeology, 11-27.

Takasu, T. 2013. RTKLIB ver. 2.4. 2 Manual. RTKLIB: An Open Source Program Package for GNSS Positioning, 29, 49.

Chapter 5: Discussion

5.1 Objectives of the thesis

This thesis investigated combining the strengths of hydroacoustic (reliable positioning and bathymetry) with underwater photogrammetry (high dense point cloud and colour image) techniques for mapping the seafloor. The objectives were:

- Objective 1: Evaluate the use of multibeam and underwater photogrammetry.
- Objective 2: Development of a portable calibration frame for underwater photogrammetry surveys.
- Objective 3: Development of a low-cost, open-source acquisition system and platform.
- Objective 4: Develop a new workflow and platform for underwater photogrammetry surveys.

These objectives were documented in the preceding chapters. This chapter discusses each objective's successes and limitations, the significance of the Thesis, identifies limitations and areas for further investigation.

5.2 Evaluating the use of multibeam and underwater photogrammetry

The Thesis commenced with a critical examination of multibeam and underwater photogrammetry techniques (Chapter 1). This chapter served as the foundation to the Thesis, by assessing the strengths and limitations of existing approaches, and (like other studies) identified benefits to combining these techniques. In summary, hydroacoustic surveys reliably provide accurate bathymetry; however, expensive systems, like multibeam echosounders, are required for high spatial resolution. Although acoustic backscatter can be used to infer the seafloor substrate, it is typically not as informative as a colour image. In comparison, underwater photogrammetry provides a simpler and more cost-effective solution to produce a higher resolution point cloud, while also producing a comprehensive orthoimage. However, the scale and positional accuracy of 3D models and orthoimages produced by underwater photogrammetry can be more challenging than for hydroacoustic surveys.

The proposed solution involved collecting position, motion, and single beam echosounder data alongside photos, all referenced to a rigid underwater frame. This integrated approach aimed to merge the advantages of hydroacoustic surveys' positional and depth accuracy with the detailed visual information from underwater photogrammetry. Additionally, Chapter 1 identified camera calibration as a key aspect to an accurate photogrammetry survey. Hence, it was this aspect was first investigated, in Chapter 2.

5.3 Development of a portable calibration frame for underwater photogrammetry surveys

The aim of Chapter 2 was to develop and evaluate a camera calibration frame designed for underwater photogrammetry surveys that could be collapsible and easily replicated by other users. The utilisation of photogrammetry has witnessed a surge across various disciplines, with marine science being no exception. A critical factor influencing the accuracy of the generated 3D models from images lies in the calibration quality and the camera's stability employed for image capture (Helmholz & Lichti, 2019). The calibration process necessitates an optimal 3D geometry to minimise correlations between the camera's interior orientation parameters. Different calibration frames are typically employed, but their practical use becomes challenging in underwater environments. These frames can be bulky, posing difficulties in handling and transportation, particularly in boat settings where space is a premium. This study addresses these challenges by aiming to develop a collapsible and portable calibration frame, specifically tailored for marine field data capture.

The proposed collapsible calibration frame, with 3D printable joints, underwent in-air and underwater validation, encompassing three comprehensive tests. The first test focused on validating the reliability of the frame, ensuring that it can be assembled in a manner that maintains the unchanged positions of Ground Control Points (GCPs) relative to each other. Despite a small bias observed, the study demonstrated that this bias can be rectified through a baseline assessment. The second test delved into repeatability, assessing whether consistent results can be achieved using the same baselines with different software and camera combinations. While a downward trend is noted for lower-grade cameras, adjustments with various software solutions and cameras affirm the frame's suitability for in-air applications.

Chapter 2 culminated with an underwater performance test, confirming the frame's usability with root-mean-squared error values below 2 mm when utilising baselines. This study achieved better results using Context Capture than MetaShape. Nevertheless, overall, it can be concluded that the results are acceptable for both cameras and software solutions. This underscores the practicality and effectiveness of the collapsible calibration frame, even in challenging underwater conditions. By addressing the limitations of traditional calibration frames and offering a portable alternative, this research contributes to advancing the capabilities of photogrammetry in marine science, facilitating more efficient and versatile data capture in marine environments. Files for the 3D printable joints are freely available to other researchers (Curtin, 2023). However, as seen in Chapter 4, the collapsable frame was outperformed by a rigid frame. This is discussed in section 5.5.

5.4 Development of a low-cost, open-source acquisition system and platform

The aim of Chapter 3 was to develop and evaluate a low cost, open-source data logging device and survey platform to collect position and depth data that could be used for underwater photogrammetry surveys. Sensors were mounted on a rigid frame and integrated with a Raspberry Pi for data logging that was put in waterproof housing. The validation and assessment of the platform focused on the performance of its position and depth sensors: an echosounder and laser distance measurer.

Evaluation of the position solutions available, namely: GPS, Precise Point Positioning (PPP), and Post-Processed Kinematic (PPK) technique, revealed that PPK was the most accurate. PPK achieved an RMS of less than 30 cm in its X-Y coordinated when compared to RTK positions. The study did investigate developing RTK capability, but the solutions available were either too expensive, or required more time to develop than available to complete the study. Nevertheless, the accuracy offered by the PPK solution was considered acceptable to fulfil the study's objective, so this was used as part of the workflow adopted in Chapter 4.

The bathymetry data processed from the position and echosounder data collected by the Rasberry Pi on the platform agreed with historic Lidar and RTK Rover data, giving confidence to the device's ability to collect accurate bathymetry. As part of Chapter 3, a green laser distance measurer was integrated into the system and evaluated as a method for measuring depth, and to create Ground Control Points, as the laser would be identifiable on the photos. Although the measurements made by the laser were found to correlate with the echosounder (after correction for refraction of light), it only worked to depths between 25 and 60 cm – and only consistently from white or near white reflectors – due to attenuation of light. Therefore, only the echosounder was used for the workflow used in Chapter 4. Further studies could investigate other lasers with higher power.

Overall, the platform was shown it could be reliably used to collect accurate position and bathymetry data in a marine setting. Additionally, it allowed camera height to be measured using pressure or PPK derived height, and the altitude using the echosounder. However, the motion sensor that had been integrated into the platform was not formally evaluated, which in hindsight is something would have been useful for Chapter 4. In Chapter 3, a swimmer was used to move the platform, tests with it being towed by an Autonomous Surface Vessel (ASV) were carried out (Figure 5.1). However, an ASV was not available for Chapter 4.

Figure 5. 1. Survey platform with logging device being pulled by an Autonomous Surface Vessel provided by Peter McKewan from PESAC Pty Ltd.

5.5 A novel workflow and platform for underwater photogrammetry surveys

The aim of Chapter 4 was to use the calibration frame (developed in Chapter 2) to calibrate three GoPro 5 cameras that were rigidly mounted to the survey platform (developed in Chapter 3), to carry out an underwater photogrammetry survey, and evaluate the position and scaling accuracy of the orthoimages and 3D models produced, using different constraints. The evaluation was carried out

over some artificial reefs located off the coast of Coogee, Western Australia. Comparison of outputs was made with aerial orthoimage and multibeam data, gridded to 10 cm, collected two years prior (in 2021) by the West Australian government.

5.5.1 Positional accuracy

In Chapter 4, three methods were considered to tag photos with the camera height: elevation of the cameras using the pressure sensor corrected for tide, elevation of the cameras using PPK derived height, and altitude to the camera using the echosounder data, all re AHD. It was found the most accurate methods were using the PPK height, and tide corrected pressure, with the later favoured due to overall agreement of DTM surfaces produced. Using altitude (derived from the single beam echosounder) as the camera's height in the photogrammetry workflow produced a 3D model with large difference from the multibeam surface, possibly as the software is effectively calculating altitude and assumes the camera height provided is the elevation. However, the single beam echosounder data was found to be effective at evaluating the height of 3D models, as it was highly correlated with the multibeam data. As a result, it was shown that where photogrammetry 3D models produced were not in agreement the multibeam bathymetry, they could be corrected to be more in agreement using the single beam bathymetry using linear regression.

Using the outlines of the artificial reefs, the X-Y positions of the orthoimage and 3D models produced using photos tagged with the PPK X-Y positions and depths using the tide corrected pressure, was found to be within 30-50 cm of the multibeam data. This difference was comparable to the positional accuracy of the PPK X-Y positions found in Chapter 3. Comparison with the orthoimage was done qualitatively, as not all reefs were visible, and it was uncertain whether the aerial image had been corrected for refraction through the water.

The PPK accuracy obtained in this Thesis are comparable to other studies, such as Di et al. (2023), who assessed a cost-effective GNSS-PPK buoy for sea surface height measurements. In the Di et al. (2023) study, single-frequency PPK resulted in errors of 0.19 cm (East), 0.30 cm (North), and 0.57 cm (vertical), with a baseline measurement error of 0.29 cm. Dual-frequency PPK showed horizontal

errors of 0.17 cm (East) and 0.25 cm (North), vertical error of 0.50 cm, and a baseline measurement error of 0.16 cm.

The IHO (International Hydrographic Organization) (2020), say the acceptable Total Horizontal Uncertainty (THU) for Post-Processed Kinematic (PPK) positioning varies according to the application. In accordance with high-precision surveying norms, aiming for centimetre-level accuracy, the recommended THU for PPK typically falls within the range of 1 to 5 cm, which the developed system falls short of using the current GNSS-PPK solution. However, the results presented here are compliant for applications with less stringent precision requirements, such as general navigation or mapping, where an acceptable THU might extend to a few meters, typically ranging from 2 to 10 m (IHO, 2020); and for environmental monitoring scenarios within shallow waters, an acceptable THU could be broader, ranging from 5 to 20 m (IHO, 2020).

This study was focused on evaluating how well the platform and workflow could perform independently. However, further work could investigate if the positional accuracy could be improved through creating GCPs using aerial photo (X-Y), or multibeam (X, Y, Z), as other studies have shown (Joo et al., 2020). However, a limitation of the study is the comparison was made using data captured two years prior, and the seafloor is a dynamic environment capable of changes within and between years (Favali & Beranzoli, 2006; Goertz & Wuestefeld, 2018), which means this would also affect how useful this data is for evaluation and integration.

5.5.2 Calibration and scaling

In Chapter 4, three types of camera calibration were evaluated: self-calibration by the (Context Capture) software using data from the survey, calibration using images captured of a standard rigid calibration (cube) frame, and calibration using images captured of the collapsible calibration frame developed in Chapter 2. While the collapsible frame was found to provide acceptable results (RMS = 2.05 pixels), the rigid cube frame was found to produce the most accurately scaled 3D models (RMS = 1.4 pixels). Self-calibration was found to result in a less accurately scaled model (RMS with multibeam = 28 cm) compared to calibration with a frame (RMS with multibeam = 17.9 cm) and showed clear artefacts such as “bowing” of the surfaces. Possible reasons for the collapsible frame

not performing as well as it did in Chapter 2 include: it is not as reproducible as initially hoped, and/or not enough coverage of images from all cameras was collected over the frame. Regardless, Chapter 4 highlighted a successfully scaled 3D models require sufficient images to be collected over a dedicated calibration frame that ensure the cameras interior orientation parameters are adequately calculated. In Chapter 4, calibration data was collected in-situ as part of the survey. Future studies could investigate the performance of camera calibration when images are not captured in-situ, as this would reduce the uncertainty of the scale accuracy of a survey, and time required to complete a survey.

5.5.3 Motion data

In Chapter 4, it was found that incorporating IMU motion sensor data did not significantly improve the accuracy of the 3D models produced. The reasons for this could be that the photogrammetry software (context capture) does a better job at determining the camera's attitude than the motion sensor used in this study, and time synchronisation is not adequate. The IMU used was an entry level sensor, with the heading derived from a magnetic compass, so further studies should investigate the performance of higher accuracy sensors, such as a dual GNSS antenna for accurate heading, and GNSS infused attitude (Huang et al., 2023; Maarse et al., 2016). In addition, while sensor data were synchronised to each other as they were integrated with the Rasberry Pi, the cameras were independent and could only be synchronised to within 1s. Future studies should investigate synchronisation of image acquisition to sensor data to reduce latency e.g. ~1 ms.

5.5.4 Coverage and resolution

Chapter 4 used two subsets of a survey of part of the Coogee Maritime Trail, whose areas were 193 m^2 (Site 1) and 90 m^2 (Site 2). The whole survey covered 10,000 m^2 (0.01 km^2) over 3 hours, i.e. a mapping speed of 3,333 m^2/hour. The average platform speed was 0.3 m/s (and a maximum = 0.5 m/s). At the same average speed, a multibeam survey (with a 120˚swath) would have a mapping speed of 3,780 m^2/hour in 1 m depth and 18,900 m^2/hour in 5 m (assuming 100% coverage). However, it is unlikely that the resulting DSM would have the same resolution (1 cm). Although the survey was successfully carried out using a swimmer to move the platform, it would have been more efficient to use an ASV, but this would add to the cost of the survey. Nevertheless, for large surveys ASVs are

likely to make surveys like this more cost effective, especially compared to a multibeam survey; and an ASV is likely to have a longer duration than in comparison to aerial drone surveys (Pieterkosky et al., 2017).

The survey was carried out in water depths between 1 and 5 m. The maximum depth achievable with this platform and workflow was not investigated as part of this study but will likely be influenced by camera selection and water clarity. Some (exploratory) side-by-side imagery was captured using a Sony RX0 ii to compare with the GoPro 5s used in Chapter 4 (Figure 5.2), which indicated cameras with a larger sensor size could offer clearer imagery a higher maximum depth. Future studies could investigate the maximum depth for different camera water conditions.

Figure 5. 2: Photo of a Abitat artificial reef at a depth of 5 m, captured on 26th August 2023 with: GoPro 5 (left) and Sony RX0 ii (right).

5.5.5 Computation

The photogrammetry processing was carried out using Context Capture on a high-performance computer system Curtin University's 3D Hub, Table 1.1 shows its key specifications. Without access to such a high-performance computer, completion of the Thesis would have been very challenging, as it reduced processing time, which allowed for experimentation of input parameters and workflow. Nevertheless, subsets of the survey were chosen as different datasets with different constraints were needed to be run. Other studies have identified computation required by photogrammetry and availability infrastructure as a bottle neck, and it is an area of active research ((Previtali et al., 2020).

Table 5. 1. Key specifications of Curtin University's 3D Hub computer system.

Parameter	**Specification**
Processing Speed	Processor: Intel Gold 6248R CPU @ 3.00GHz, 2993 MHz, 24 Core(s), 48 Logical Processor(s)
Installed Physical Memory (RAM)	512 GB
OS Name	Microsoft Windows 10 Pro for Workstations

5.6 Significance of the thesis

The Thesis developed a new camera calibration frame and data logging device and platform system to carry out underwater photogrammetry surveys of shallow coast water environments, with the aim of producing high-resolution (1 cm), accurately scaled (RMS < 0.2 m) and geo-referenced (RMS < 0.3 m) orthoimages and 3D models of the seafloor. Figure 3 shows example outputs of the Thesis compared to traditional methods to collect these data. This workflow and platform has several distinct advantages in underwater mapping compared to traditional methods used to collected orthoimages and bathymetry.

In shallow water coastal areas, bathymetric lidar or multibeam echosounders are typically used to obtain high-resolution bathymetry. In the study area, the available bathymetry was a 5 m grid from a Lidar survey and a 1 m multibeam survey (which was re-gridded to 10 cm). This workflow and platform here was able to produce higher resolution bathymetry maps (for the water depth) that were similar in their accuracy and geo-referencing accuracy (Figure 5.3), especially considering the cost of the proposed setup is much lower than either of those methods. In addition, although LiDAR and multibeam surveys can produce a backscatter intensity image to infer seafloor substrate, the orthoimages produced from photogrammetry offer much more detail.

Orthoimages can be created from aerial and ROV/AUV photogrammetry surveys. The proposed methodology offers advantages to aerial photogrammetry, namely higher resolution, no refraction, and no obstruction from sun-glint from or waves at the water surface. Although aerial platforms with a higher coverage and mapping speed, if the proposed setup is operated by an ASV it is likely to have a higher endurance. Compared to using a diver or an ROV or AUV, the methods presented in

this Thesis have higher positioning accuracy. In addition, the use of the Echosounder gave a method for validation and (if necessary) to align to a vertical datum more accurately.

While showcasing promising advantages, the new underwater mapping system is not without its limitations, and understanding these constraints is essential for realistic expectations and effective utilisation. One notable limitation is the maximum water depth within which the system can operate optimally. However, there are a variety of valuable applications like habitat mapping, archaeological surveys, and nearshore environmental monitoring, where a comprehensive understanding of the underwater landscape is paramount. In addition, this method might also be used in deeper water to create GCPs for AUV/ROV surveys.

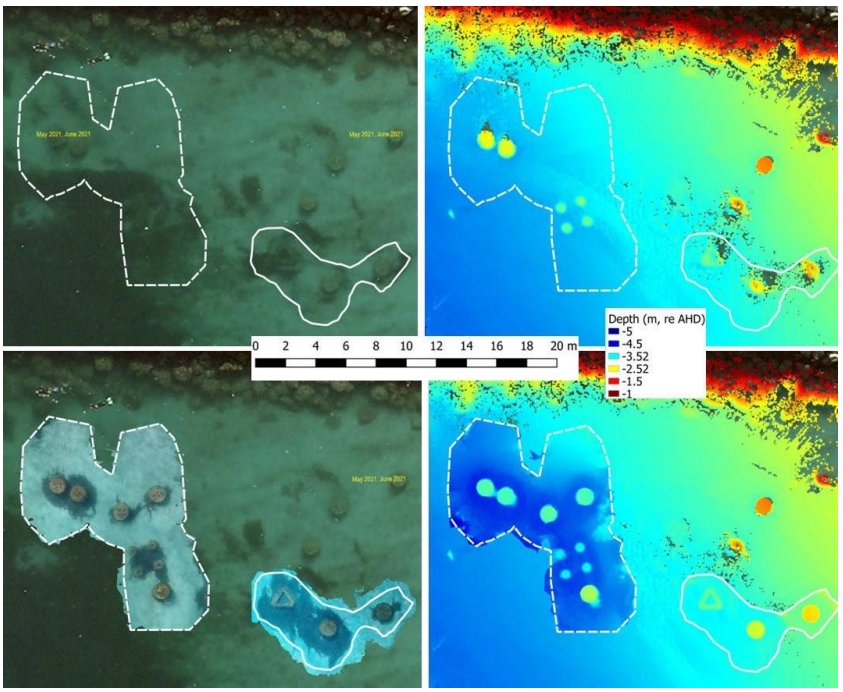

Figure 5. 3. Example outputs of Thesis (indicated by the white polygons) compared with traditional methods: aerial photo (10 cm) without (top left) and with underwater orthoimage (1 cm) produced over the top (bottom left); multibeam bathymetry (10 cm) without (top right) and with DSM (1 cm) produced over the top (bottom right).

5.7 Recommendations

5.7.1 Workflow

Overall, the results of Chapter 4 showed that accurate, high-resolution orthoimages and 3D models of the seafloor could be collected between 1 and 5 m depth, using the recommended workflow:

1) Pre-survey camera calibration using a frame allowing a full range of images capture, with a rigid frame produced the most accurate results, the collapsible frame developed here was shown to produced comparable results when sufficient images are captured and using baselines.
2) Images to be synchronized and tagged with accurate X, Y, Z positions, e.g., using PPK, and pressure to measure the camera height.
3) Hydo-acoustic data to be collected, ideally simultaneously, to allow direct validation, and where necessary adjusted to be more aligned with the true location of the seafloor relative to a vertical datum.

5.7.2 Future studies

Various recommendations were also identified for future studies to develop this area further, in summary these are to investigate:

- Better specification sensors and cameras
- Using an ASV for data capture
- Pre-survey calibrations
- Computational options

It is likely the integration of RTK positioning and GNSS-fused attitude will improve the georeferencing, but this will come at a higher cost. Higher specification cameras (resolution, sensor size, pixel size, and lens) will provide better images and likely a higher maximum depth operation, but new cameras will require testing for stability (Helmholz et al, 2016). Although using an ASV would be more expensive, it would increase the survey endurance thereby allowing more coverage, and an autopilot system would allow for effective line planning so there are no holes in coverage. Although in-situ is recommended, ex-situ camera calibration processing would increase survey efficient and reduce uncertainty and is worth.

investigation. Computation required for photogrammetry is quite high, so any development of software or hardware making this process quicker and/or more accessible.

Reference

Addona, F., Sistilli, F., Romagnoli, C., Cantelli, L., Liserra, T., & Archetti, R. (2022). Use of a Raspberry-Pi Video Camera for Coastal Flooding Vulnerability Assessment: The Case of Riccione (Italy). Water, 14(7), 999.

Agrafiotis, P., Karantzalos, K., Georgopoulos, A., & Skarlatos, D. (2020). Correcting image refraction: Towards accurate aerial image-based bathymetry mapping in shallow waters. Remote Sensing, 12(2), 322.

Balletti, C., Beltrame, C., Costa, E., Guerra, F., & Vernier, P. (2015). Underwater Photogrammetry and 3D Reconstruction of Marble Cargos Shipwreck. International Archives of the Photogrammetry, Remote Sensing & Spatial Information Sciences.

Barrile, V., Fotia, A., Ponterio, R., & Aliotta, F. (2019). Photogrammetric techniques for the reconstruction of underwater 3d models of seabed and artifacts. The International Archives of the Photogrammetry, Remote Sensing and Spatial Information Sciences, 42, 25-30.

Beaman, R. J., & Harris, P. T. (2005). Bioregionalization of the George V Shelf, East Antarctica. Continental Shelf Research, 25(14), 1657-1691.

Bibuli, M., Ferretti, R., Odetti, A., & Cosso, T. (2021). River Survey Evolution by means of Autonomous Surface Vehicles. 2021 International Workshop on Metrology for the Sea; Learning to Measure Sea Health Parameters (MetroSea),

Brown, C. J., Smith, S. J., Lawton, P., & Anderson, J. T. (2011). Benthic habitat mapping: A review of progress towards improved understanding of the spatial ecology of the seafloor using acoustic techniques. Estuarine, Coastal and Shelf Science, 92(3), 502-520.

Buchanan, C., Spinoccia, M., Picard, K., Wilson, O., Sexton, M., Hodgkin, S., Parums, R., Carey, M., & Siwabessy, J. Standard Operation Procedure for a Multibeam Survey.

Drap, P. (2012). Underwater photogrammetry for archaeology. Special applications of photogrammetry, 114.

Favali, P., & Beranzoli, L. (2006). Seafloor observatory science: A review. Annals of geophysic.

Gawlik, N. (2014). 3D modelling of underwater archaeological artefacts Institutt for bygg, anlegg og transport].

Goertz, A., & Wuestefeld, A. (2018). Real-time passive monitoring with a fibre-optic ocean bottom array. First Break, 36(4), 55-61.

Hedley, J. D., Roelfsema, C. M., Chollett, I., Harborne, A. R., Heron, S. F., J. Weeks, S., Skirving, W. J., Strong, A. E., Eakin, C. M., & Christensen, T. R. (2016). Remote sensing of coral reefs for monitoring and management: a review. Remote Sensing, 8(2), 118.

Helmholz, P., & Lichti, D. (2019). Assessment of chromatic aberrations for gopro 3 cameras in underwater environments. ISPRS Annals of the Photogrammetry, Remote Sensing and Spatial Information Sciences, 4, 575-582.

Helmholz, P., Long, J., Munsie, T., & Belton, D. (2016). ACCURACY ASSESSMENT OF GO PRO HERO 3 (BLACK) CAMERA IN UNDERWATER ENVIRONMENT. International Archives of the Photogrammetry, Remote Sensing & Spatial Information Sciences, 41.

Huang, S.-E., Chang, P.-H., Lu, X.-L., & Juang, J.-C. (2023). A Satcom On-the-Move Phased-Array Antenna Tracking Algorithm on Robot Operating System. 2023 23rd International Conference on Control, Automation and Systems (ICCAS),

International Hydrographic Organisation, IHO S-44, "Standards for Hydrographic Survey", 6th Edition, September, 2020, International Hydrographic Bureau, Monaco.

Instruments, L.-C. S. (2000). Multibeam Sonar Theory of Operation.

Kawamura, Y., Tahara, J., Kato, T., Fujii, S., Baba, S., & Koike, M. (2021). Development of small autonomous surface vehicle implementing position control system using sliding mode control. Sens Mater, 33(3), 883-895.

Kenny, A. J., Cato, I., Desprez, M., Fader, G., Schüttenhelm, R., & Side, J. (2003). An overview of seabed-mapping technologies in the context of marine habitat classification. ICES Journal of Marine Science, 60(2), 411-418.

Kılınç Kazar, G., Karabörk, H., & Makineci, H. B. (2022). Evaluation of test field-based calibration and self-calibration models of UAV integrated compact cameras. Journal of the Indian Society of Remote Sensing, 50(1), 13-23.

Kostylev, V. E., Todd, B. J., Fader, G. B., Courtney, R., Cameron, G. D., & Pickrill, R. A. (2001). Benthic habitat mapping on the Scotian Shelf based on multibeam bathymetry, surficial geology and sea floor photographs. Marine Ecology Progress Series, 219, 121-137.

Lamarche, G., Orpin, A. R., Mitchell, J. S., & Pallentin, A. (2016). Benthic habitat mapping. Biological sampling in the deep sea, 80-102.

Lubczonek, J., Kazimierski, W., Zaniewicz, G., & Lacka, M. (2021). Methodology for combining data acquired by unmanned surface and aerial vehicles to create digital bathymetric models in shallow and ultra-shallow waters. Remote Sensing, 14(1), 105.

Luhmann, T., Fraser, C., & Maas, H.-G. (2016). Sensor modelling and camera calibration for close-range photogrammetry. ISPRS Journal of Photogrammetry and Remote Sensing, 115, 37-46.

Malthus, T. J., & Mumby, P. J. (2003). Remote sensing of the coastal zone: an overview and priorities for future research.

Manoukian, S., Fabi, G., & Naar, D. F. (2011). Multibeam investigation of an artificial reef settlement in the adriatic sea (Italy) 33 years after its deployment. Brazilian Journal of oceanography, 59, 145-153.

Missiaen, T., Sakellariou, D., & Flemming, N. C. (2017). Survey strategies and techniques in underwater geoarchaeological research: An overview with emphasis on prehistoric sites. Under the sea: Archaeology and palaeolandscapes of the continental shelf, 21-37.

Morel, T. A., Manzano, J. M., Bejarano, G., & Orihuela Espina, D. L. (2022). Modelling and identification of an autonomous surface vehicle: Technical report.

Parnum, I., & Gavrilov, A. (2012). High-frequency seafloor acoustic backscatter from coastal marine habitats of Australia. Proceedings fo the Australian Society of Australia.

Pickrill, R. A., & Todd, B. J. (2003). The multiple roles of acoustic mapping in integrated ocean management, Canadian Atlantic continental margin. Ocean & Coastal Management, 46(6-7), 601-614.

Pieterkosky, S., Ziegwied, A., Cavanagh, C., & Thompson, L. (2017). BIV meets ASV: Bio-inspired fish drones and autonomous surface vehicles for coral reef monitoring. OCEANS 2017-Anchorage,

Pittman, S. J., Costa, B. M., & Battista, T. A. (2009). Using lidar bathymetry and boosted regression trees to predict the diversity and abundance of fish and corals. Journal of Coastal Research(10053), 27-38.

Previtali, M., Brumana, R., & Banfi, F. (2020). Existing infrastructure cost effective informative modelling with multisource sensed data: TLS, MMS and photogrammetry. Applied Geomatics, 1-20.

Roman, C., Inglis, G., & Rutter, J. (2010). Application of structured light imaging for high resolution mapping of underwater archaeological sites. OCEANS'10 IEEE SYDNEY,

Sabol, B. M., Eddie Melton, R., Chamberlain, R., Doering, P., & Haunert, K. (2002). Evaluation of a digital echo sounder system for detection of submersed aquatic vegetation. Estuaries, 25(1), 133-141.

Shortis, M. R., Miller, S., Harvey, E., & Robson, S. (2000). An analysis of the calibration stability and measurement accuracy of an underwater stereo-video system used for shellfish surveys. Geomatics Research Australasia, 1-24.

Vargas, S. M., Vitale, A. J., Genchi, S. A., Nogueira, S. F., Arias, A. H., Perillo, G. M., Siben, A., & Delrieux, C. A. (2023). Monitoring multiple parameters in complex water scenarios using a low-cost open-source data acquisition platform. HardwareX, 16, e00492.

Woodget, A., Carbonneau, P., Visser, F., & Maddock, I. P. (2015). Quantifying submerged fluvial topography using hyperspatial resolution UAS imagery and structure from motion photogrammetry. Earth surface processes and landforms, 40(1), 47-64.

Appendix: A

Mufti, A., Parnum, I., Belton, D., & Helmholz, P. (2019). Investigation of in-field devices for underwater surveying of reef structures. Poster presented at the Australian Marine Science Association conference, Fremantle, Western Australia, 7-11 July 2019.

1) Centre for Marine Science and Technology, Curtin University, Bentley, Western Australia
2) School of Earth and Planetary Science, Curtin University, Bentley, Western Australia

Investigation of in-field devices for underwater surveying of reef structures

Alaa Mufti[1,2], Iain Parnum[1,2], David Belton[2] and Petra Helmholz[2]

Introduction

The aim of this study is to investigate how accurate and precise in-field devices at measuring underwater structures and features. These methods will be tested on a structure with well a known structure, where it has been directly (physically) measured or fabricated with known specifications, such as an Artificial Reef. This poster presents the results of the first data collection with a multibeam echo-sounder system over two pre-fabricated Artificial Reefs structures located 11 km south of the west end of Rottnest Island, Western Australia. As the structure and dimensions are well understood through engineering diagrams, they provide a valuable test site for underwater survey methods. Future work will include mapping the structures with other techniques, such as photogrammetry and laser, as well as repeating surveys to examine precision.

Methods

A multibeam survey was carried out on 27th September 2018 using the Western Australia Department of Transport's (DoT) hydrographic vessel the Alec Hansen lll. Data were collected over the artificial reef structures with DoT's R2Sonic 2024 multibeam echo-sounder and Applanix POS MV for position and attitude data. Acquisition was carried out in QPS QINSy. Post-processing of the POS MV data was carried out using Applanix POS Pac MMS. Processing of the bathymetry was carried out in QPS QIMERA. Engineering diagrams were drawn in Autodesk AutoCAD, and the point cloud was created in the Autodesk ReCap. Comparison between the multibeam measurements and the engineering diagram was carried out in CloudCompare including calculating the Root-Mean-Square (RMS) difference between the multibeam measurements and diagram.

Results

A 1m grid of the multibeam bathymetry surface can be seen in a 2D view in Figure 1 and a 3D view in Figure 2. A 3D view of the multibeam point cloud over the engineering diagram can be seen in Figure 3.

Results

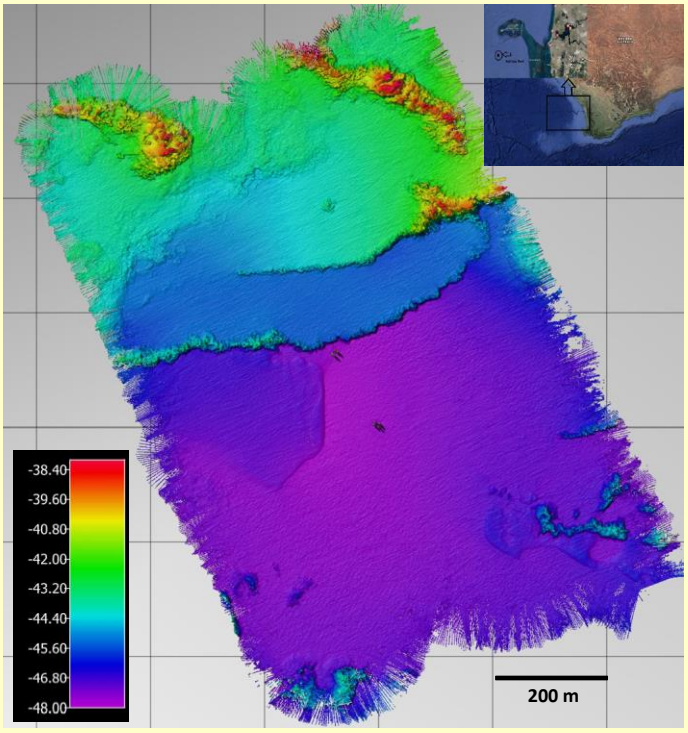

Figure 1: 2D View of the bathymetry of the Artificial Reefs and surrounding area.

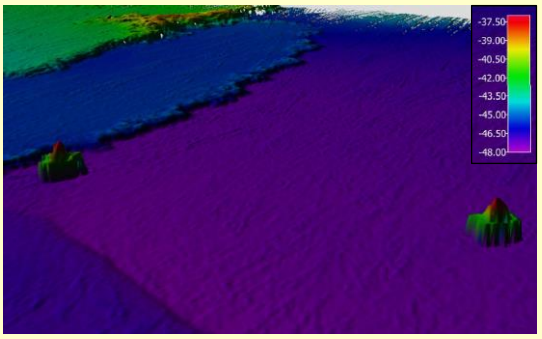

Figure 2: 3D View of the of the Artificial Reefs.

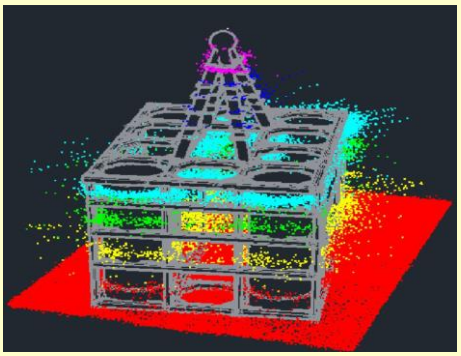

Figure 3: 3D View of the of the multibeam-measured point cloud over the engineering diagram of the Artificial Reef.

Analysis

Using the reef structures, the dynamic offsets of the multibeam system were further improved by the addition of –0.957° in the pitch alignment (Figure 4). The unsigned distances between the multibeam point cloud and the engineering diagram are shown as a 3D view (Figure 5) and signed values as a histogram (Figure 6). The RMS between the multibeam measurements and the engineering diagram was 1.167 m. The mean signed distribution distance was 0.846 m, and standard deviation was 0.939 m. However, the seafloor has contributed to the high distances see in Figures 5 and 6. Future work will aim to remove these points from the analysis.

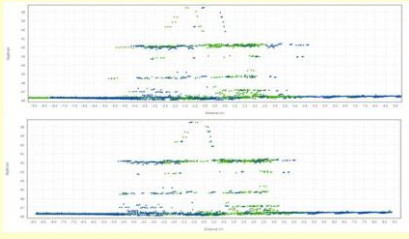

Figure 4: Point clouds over part of the Artificial reef: before (top) and after (bottom) adjusting the pitch offset.

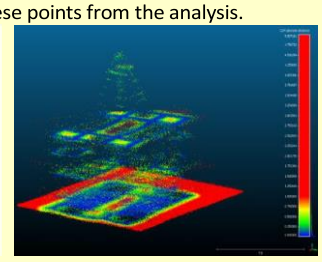

Figure 5: Unsigned distance between the multibeam point cloud and the diagram.

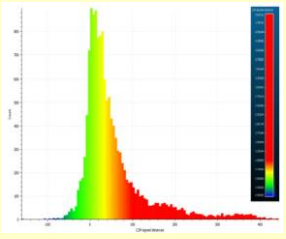

Figure 6: Histogram of the signed distances between the multibeam point cloud and diagram.

Acknowledgements

The authors would like to thank West Australian Department of Transport for their support by providing a vessel, skipper and multibeam mapping system, in particular: John Mullally, Kim Edwards and Ralph Talbot-Smith. Thanks also to RecFishWest for information about the Artificial Reef Structures, in particular: Stephanie Watts and Matt Gillett.

Government of **Western Australia**
Department of **Transport**

Appendix: B

Attribution statement

Chapter 2: Introduction and validation of a novel calibration frame

Alaa Mufti, Petra Helmholz, Iain Parnum, David Belton

	Conception and Design	Acquisition of Data and Method	Data Conditioning and Manipulation	Analysis and Statistical Method	Interpretation and Discussion
Co-author 1 Alaa Mufti	50%	60%	60%	60%	50%
Co-author 1 acknowledgment: I acknowledge that these represent my contribution to the above research output, and I have approved the final version. Signature: Alaa Mufti					
	Conception and Design	Acquisition of Data and Method	Data Conditioning and Manipulation	Analysis and Statistical Method	Interpretation and Discussion
Co-author 2 Petra Helmholz	20%	20%	30%	20%	20%
Co-author 2 acknowledgment: I acknowledge that these represent my contribution to the above research output, and I have approved the final version. Signature: Petra Helmholz					
	Conception and Design	Acquisition of Data and Method	Data Conditioning and Manipulation	Analysis and Statistical Method	Interpretation and Discussion
Co-author 3 Iain Parnum	10%	20%	10%	20%	20%
Co-author 3 acknowledgment: I acknowledge that these represent my contribution to the above research output, and I have approved the final version. Signature: Iain Parnum					
	Conception and Design	Acquisition of Data and Method	Data Conditioning and Manipulation	Analysis and Statistical Method	Interpretation and Discussion
Co-author 4 David Belton	20%	x	x	x	10%
Co-author 4 acknowledgment: I acknowledge that these represent my contribution to the above research output, and I have approved the final version. Signature:					

Chapter 3: An open-source, data logging device for marine-based surveys

Alaa Mufti, Iain Parnum, David Belton, Petra Helmholz

	Conception and Design	Acquisition of Data and Method	Data Conditioning and Manipulation	Analysis and Statistical Method	Interpretation and Discussion
Co-author 1 Alaa Mufti	50%	50%	50%	50%	50%
Co-author 1 acknowledgment: I acknowledge that these represent my contribution to the above research output, and I have approved the final version. Signature: Alaa Mufti					
	Conception and Design	Acquisition of Data and Method	Data Conditioning and Manipulation	Analysis and Statistical Method	Interpretation and Discussion
Co-author 2 Iain Parnum	40%	40%	40%	40%	20%
Co-author 2 acknowledgment: I acknowledge that these represent my contribution to the above research output, and I have approved the final version. Signature: Iain Parnum					
	Conception and Design	Acquisition of Data and Method	Data Conditioning and Manipulation	Analysis and Statistical Method	Interpretation and Discussion
Co-author 3 David Belton	10%	10%	10%	10%	10%
Co-author 3 acknowledgment: I acknowledge that these represent my contribution to the above research output, and I have approved the final version. Signature: DBelton					
	Conception and Design	Acquisition of Data and Method	Data Conditioning and Manipulation	Analysis and Statistical Method	Interpretation and Discussion
Co-author 4 Petra Helmholz	x	x	x	x	20%
Co-author 4 acknowledgment: I acknowledge that these represent my contribution to the above research output, and I have approved the final version. Signature: Petra Helmholz					

Chapter 4: A novel workflow and platform for underwater photogrammetry surveys

Alaa Mufti, Petra Helmholz, David Belton, Amir Allahvirdizadeh, Iain Parnum

	Conception and Design	Acquisition of Data and Method	Data Conditioning and Manipulation	Analysis and Statistical Method	Interpretation and Discussion
Co-author 1 Alaa Mufti	50%	50%	50%	50%	50%
Co-author 1 acknowledgment: I acknowledge that these represent my contribution to the above research output, and I have approved the final version. Signature: Alaa Mufti					
	Conception and Design	Acquisition of Data and Method	Data Conditioning and Manipulation	Analysis and Statistical Method	Interpretation and Discussion
Co-author 2 Petra Helmholz	20%	x	20%	20%	20%
Co-author 2 acknowledgment: I acknowledge that these represent my contribution to the above research output, and I have approved the final version. Signature: Petra Helmholz					
	Conception and Design	Acquisition of Data and Method	Data Conditioning and Manipulation	Analysis and Statistical Method	Interpretation and Discussion
Co-author 3 David Belton	5%	15%	10%	10%	5%
Co-author 3 acknowledgment: I acknowledge that these represent my contribution to the above research output, and I have approved the final version. Signature: Amir Allahvirdizadeh					
	Conception and Design	Acquisition of Data and Method	Data Conditioning and Manipulation	Analysis and Statistical Method	Interpretation and Discussion
Co-author 4 Amir Allahvirdizadeh	5%	5%	x	x	5%
Co-author 5 acknowledgment: I acknowledge that these represent my contribution to the above research output, and I have approved the final version. Signature: DBelton					
	Conception and Design	Acquisition of Data and Method	Data Conditioning and Manipulation	Analysis and Statistical Method	Interpretation and Discussion
Co-author 5 Iain Parnum	20%	30%	20%	20%	20%
Co-author 4 acknowledgment: I acknowledge that these represent my contribution to the above research output, and I have approved the final version. Signature: Iain Parnum					